The Adsorption Properties of Microporous Activated Carbon Prepared from Pistachio Nut Shell for Low Concentration VOCs Under Low-medium Temperatures

Tangying Cheng
Southeast University
Jinjin Li
Southeast University
Xiuwei Ma
Southeast University
Lei Zhou
Nanchang Hangkong University
Hao Wu
Nanjing Normal University
Linjun Yang (ylj@seu.edu.cn)
Southeast University

Research Article

Keywords: VOCs, activated carbon, pistachio-nut shell, biochar, adsorption, boiling point

Posted Date: March 22nd, 2021

DOI: https://doi.org/10.21203/rs.3.rs-323143/v1

Version of Record: A version of this preprint was published at Environmental Science and Pollution Research on July 6th, 2021. See the published version at https://doi.org/10.1007/s11356-021-14586-y.

The adsorption properties of microporous activated carbon prepared from pistachio nut shell for low concentration VOCs under low-medium temperatures

Tangying Cheng,[1] Jinjin Li,[1] Xiuwei Ma,[1] Lei Zhou,[2] Hao Wu[3] and Linjun Yang*,[1]

[1] Key Laboratory of Energy Thermal Conversion and Control, Ministry of Education, School of Energy and Environment, Southeast University, Nanjing, Jiangsu 210096, People's Republic of China

[2]National-Local Joint Engineering Research Center of Heavy Metals Polluants Control and Resource Utilization, College of Environmental and Chemical Engineering, Nanchang Hangkong University, Jiangxi 330063, People's Republic of China

[3]School of Energy and Mechanical Engineering, Nanjing Normal University, Nanjing, Jiangsu 210042, People's Republic of China

*Corresponding author: 101010340@seu.edu.cn

Tel.:+86-13851784679

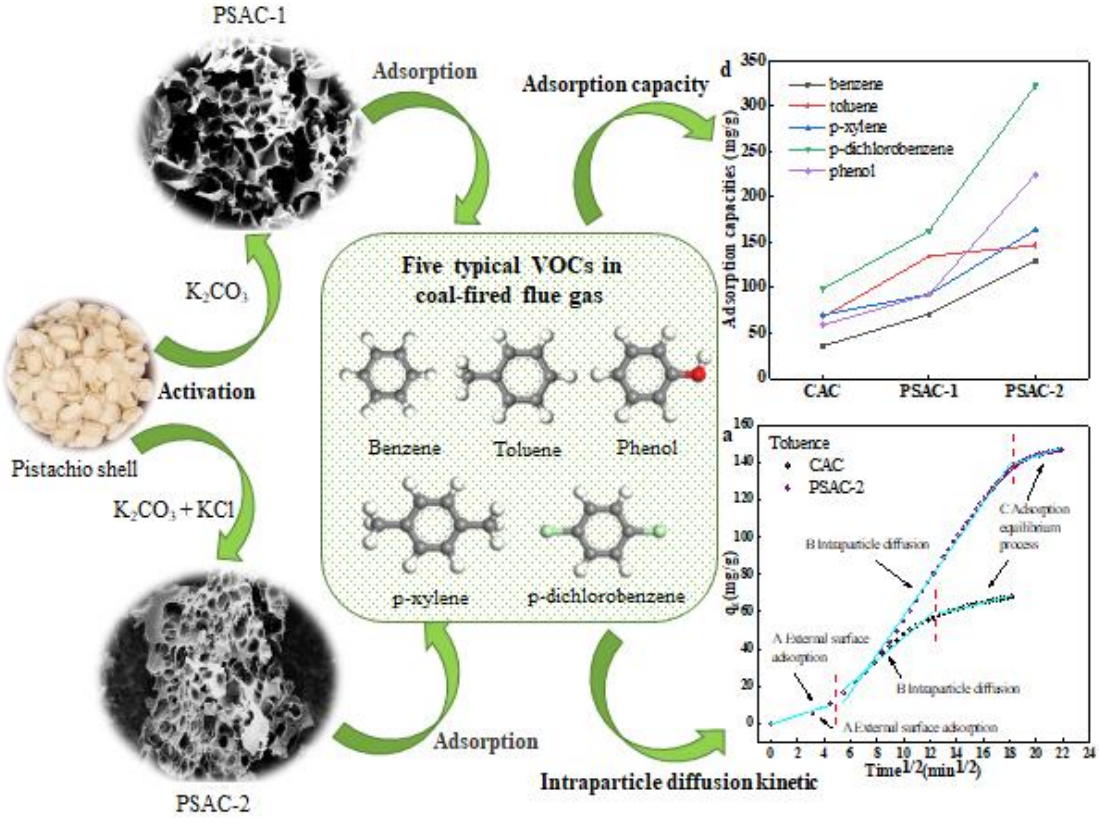

Graphical Abstract

Abstract: The control of low concentration VOCs in coal flue gas is one of the research hotspots at present. Activated carbon (AC) is often used as adsorbent for the control of VOCs due to its rich pore structure and thermal stability. In this paper, agricultural wastes pistachio shell was used as biomass AC raw materials, K_2CO_3 and KCl was used as activators. High surface area and high porosity activated carbon can be produced by the two activators used together. By comparing the differences in pore size structure and functional groups between biomass AC and commercial AC, it was found that biomass AC had better properties. The adsorption performance of different ACs on low concentration VOCs was tested at low-medium temperatures. It is concluded that biomass AC has excellent adsorption performance, and its maximum adsorption capacity can reach 3.8 times that of commercial AC. All the three adsorption kinetic models had good fitting on the adsorption process of ACs, indicating that physical adsorption is dominant in the adsorption process, while chemical adsorption existed. Using the Weber-Morris kinetic model to fit the adsorption process, it was found that the stage of external membrane mass transfer is the control stage of adsorption rate.

Key words: VOCs, activated carbon, pistachio-nut shell, biochar, adsorption, boiling point.

1. Introduction

With the continuous development of China's economy and the improvement of urbanization, VOCs emissions will continue to grow nationwide, "Fourteenth Five-Year" period, air quality to further improve, VOCs prevention is one of the "protagonists". Most VOCs with an "irritant-teratogenic-carcinogenic" characteristic are considered as precursors of ozone, dioxins and aerosols in the atmosphere, which can cause great harm to human health, plant and animal growth and ecological natural environment (Liu et al., 2020). Research have shown that VOCs in southern China mainly have the following sources, paint solvent usage, paint solvent usage + liquefied petroleum gas (LPG) usage, biomass burning, coal burning + industry combustion source, gasoline vehicle exhaust gas, diesel exhaust, industrial sources, the fuel evaporation(gasoline), the contribution rate were 11 %, 22 %, 13 %, 17 %, 12 %, 8 %, 11 %, 6 % respectively (Song et al., 2019). Compared with other sources, coal and industrial combustion sources contribute a large part to VOCs amounting to 12%, so the control of VOCs in its flue gas needs to be strengthened. Different from VOCs which is emitted by industrial production, VOCs in coal-fired flue gas have the characteristics of large gas capacity, medium-high temperature, low concentration and complex composition (Cheng et al., 2018). Therefore, although there are a large number of studies on VOCs control, most of them focus on the control of VOCs at low temperature and high concentration, while few focus on the control of middle temperature, low concentration VOCs.

The control methods of VOCs can be divided into recovery and destruction

methods, recovery methods mainly include adsorption, absorption, condensation. Destruction methods mainly include combustion, photocatalytic oxidation. Among these technologies, adsorption method is widely regarded as an effective method to remove VOCs due to its simple operation and low cost (Qu et al., 2009), activated carbon (AC) is the most common adsorbent, due to their porous structure and surface properties. However, because the price of commercial AC is relatively expensive, their use will be limited in many cases (Cardoso et al., 2008). The preparation of high-performance AC from cheap agricultural wastes such as rice husk (Liu et al., 2012), bamboo (Deng et al., 2015), coconut shell (Sarswata and Mohan, 2016), date palm root (Hadoun et al., 2013) and wood sawdust (Foo and Hameed, 2011) has become one of the research hotspots.

Pistachio-nut shell is a waste of agricultural products in recent years, its composition is: moisture 4.0 %, volatile 73.4 %, fixed carbon 21.6 %, ash 1.0 % (Foroushani et al., 2016), and pistachio factories produce nearly 1 million tons of pistachios for consumption each year (Marett et al, 2017). The shells make up a little under half of the mass of the total nut, so it is estimated that between 400,000 and 500,000 tons of pistachio shells are produced globally every year (Açıkalın et al., 2012). Numerous scholars at home and abroad have been carried out to prepare AC from pistachio-nut shell. Lua and Yang (2003, 2004a, 2004b, 2004c, 2004d, 2005, 2006) prepared AC from pistachio-nut shells between 2003 and 2009, by controlling the activation method, the activation temperature, the types of activator, pyrolysis environment, to study the structure and chemical properties of AC prepared under

different experimental factors. In addition, Kaghazchi et al. (2010) and Dolas et al. (2011) had made researches on how to prepare high specific surface area pistachio-nut shell AC, Kamandari et al. (2013, 2015), Foroushani et al. (2016), Bazan-Wozniak et al. (2017), Niksiar and Nasernejad (2017, 2018) had researched the effects of the preparation process and process parameters on the characteristics of pistachio-nut shell AC, the application of pistachio-nut shell AC had been researched by Vijayalakshmi (2010). Therefore, pistachio-nut shell is a kind of potential biomass carbon precursor.

In the course of previous research, it is known that carbonization and activation are the key factors that affect the adsorption capacity of activated carbon in the production process of activated carbon. K_2CO_3 is one of the commonly used activator due to its low cost and easier recovery. It is found that K_2CO_3 was never been used in producing pistachio shell AC, the pistachio shell AC was not applied to the control of low concentration VOCs in coal-fired flue gas, either. If the pistachio shell can be applied to the control of VOCs in coal-fired flue gas, it will not only realize the reuse of agricultural wastes, but also be significant to purify environmental pollution. This paper studied the effect of different activators on the pore structure of ACs prepared from pistachio-nut shell. The adsorption experiments of ACs on various VOCs were conducted to investigate the adsorption performance of ACs and the effect of adsorption molecular properties on the adsorption effect. The pseudo first order kinetic model, pseudo second order kinetic model, Elovich kinetic model and the Weber-Morris kinetic model were used to analyze the adsorption behavior and mechanism of VOCs on ACs. The results of this study can provide some references for the commercial production of

biomass AC and the removal of VOCs in coal-fired flue gas.

2. Experiment

2.1. Raw material

Pistachio shell was selected as the raw material to produce biomass AC. K_2CO_3 was selected as the activator for activating pistachio shell, and KCl was selected as the combined activator to investigate the adsorption effect of AC prepared by combined activation. In addition, commercial coconut shell AC, denoted as CAC, was selected for comparison. The chemical regents are all analytical grade.

Benzene, toluene, p-xylene, p-dichlorobenzene and phenol, five typical VOCs commonly found in coal-fired flue gases were selected as absorbates. Their main properties are shown in Table 1. Molecular dimension was first calculated by using Materials Studio software to draw organic molecules, and then use DMol3 method to optimize the molecular structure. Measure the bond length and bond angle of the VOCs through software, and the length and width of molecules were calculated by combining the van der Waals radius of each atom (Yang et al., 2016).

Table 1 Physical characteristics of adsorbates.

Adsorbates	MSF①	MW②	BP③	Dm④	ε_r⑤	Molecular Dimension	
						L⑥	W⑦
Benzene		78.11	80.1	0	2.274-2.292	0.7123	0.6458
Toluene		92.14	110.6	0.375	2.364-2.385	0.7251	0.6457
p-xylene		106.167	138.5	0	2.22-2.273	0.7381	0.6444
p-dichlorobenzene	 ⑧	147	174	0	2.394	0.9854	0.6447

Phenol	 ⑨	94.11	181.9	1.224	9.78-12.40	0.5874	0.6458

① MSF: molecular structural formula. ② MW: molecular weight (g/mol). ③ BP: boiling points (°C). ④ Dm: dipole moment (D=3.33564×10-30C·m). ⑤ ε_r: relative dielectric constant. ⑥ L: length (nm). ⑦ W: width (nm). ⑧ The green balls are chlorine. ⑨ The red ball is oxygen.

2.2. Preparation of pistachio shell ACs

The pistachio shell was washed by ultrapure water, dried and crushed. Then, 10 g pistachio shells and 5 g K_2CO_3 were mixed with 100 ml ultrapure water, the mixture was placed in an oven at 80 ºC for 24 h. Subsequently, the dried samples were placed in a tube furnace under nitrogen atmosphere and raised to 700 ºC at a heating rate of 10 ºC/min, held at 700 ºC for 2 hours. Washing the sample with diluted hydrochloric acid and ultrapure water until neutral filtrate and then dried it, the product was ground into powder and denoted as PSAC-1. To explore the effect of K_2CO_3 and KCl combined activation on the performance of biomass AC, in the preparation process of the above-mentioned biomass AC, 2 g KCl reagent was added in the step of adding the activator and activated together with the K_2CO_3 reagent, the subsequent steps are the same as above, and the prepared biochar is denoted as PSAC-2.

In order to better understand the activation mechanism of K_2CO_3 and KCl on pistachio shell, controlled trials were set up. 2 g KCl was used to activate pistachio nut shells without K_2CO_3, the rest of the steps were the same as above, and the product was recorded as PSAC-3. At the same time, PSAC-4 was prepared without K_2CO_3 and KCl follow the above steps.

2.3. Textural and chemical characterization

The specific surface area, pore volume and pore size distribution of AC samples were measured by automatic three-station specific surface and pore distribution instrument (Microtra BELSORP-Max, Japan). The specific surface area of the sample is calculated by the Brunner−Emmet−Teller (BET) method, and the adsorption capacity of nitrogen at relative pressure (P) P/P_0=0.99 was taken to calculate the pore volume. The Horvath-Kawazoe (HK) method and the Barrett-Joyner-Halenda (BJH) method were used to calculate the micropore pore size distribution and mesopore pore size distribution respectively. Dubinin-Astakhov (DA) method was used for linear fitting to form the characteristic curve, the DA equation is expressed as follows.

$$\log V=\log V_0-\left(\frac{A}{\beta E_0}\right)^n \quad (1)$$

$$A=RT\ln\left(\frac{P_0}{P}\right) \quad (2)$$

Where V (cm^3/g) is the adsorption capacity of P, V_0 (cm^3/g) is the adsorption capacity under saturated vapor pressure, β is the adsorption affinity coefficient, E_0 (kJ/mol) is the characteristic energy. The calculation method of the mean pore diameter of ACs (D_{AC}) is as follows (Cazorla-Amorós et al., 1998).

$$D_{AC}=\frac{10.8}{(E_0-11.4)} \quad (3)$$

The surface morphology of the sample was observed by field emission scanning electron microscope (SEM) (ULTRA PLUS-43-13, Germany). The X-ray photoelectron spectroscopy (XPS) (Thermo ESCLAB 250xi, USA) was used to determine the content of various elements on the surface of AC samples and the types and distribution of various functional groups.

2.4. VOCs adsorption test

The experimental device is shown in Fig. 1, which is mainly composed of three parts, VOCs generator, a fixed-bed and VOCs concentration detection device. VOCs gases occur through the N_2 carrier gas and N_2 balance gas two path, N_2 carrier gas is measured by mass flow meter and then enters the thermostat to take out the volatile organic vapor and mix it with N_2 balance gas in the static mixer. The concentration of VOCs gas is controlled by adjusting the inside radius of VOCs evaporate bottle mouth, the temperature of the thermostat and the amount of balance and carrier gas.

The concentration of VOCs gas is measured online by a portable total hydrocarbon analyzer equipped with a flame ionization detector (POLARIS FID 300, Italy). After passing through the static mixer, the gas is divided into two paths, one goes directly into the PF300 to measure the inlet concentration, and the other goes through the fixed-bed reactor filled with adsorbent into the PF300 to measure the outlet concentration. The saturated adsorption capacity of the adsorbent is calculated by the breakthrough curve, and the calculation formula is as follows:

$$q_e = \frac{QC_0}{1000m}\left(t_e - \int_0^{t_e} \frac{C_t}{C_0} dt\right) \quad (4)$$

Where q_e (mg/g) represents the saturated adsorption capacity of VOCs per unit mass of adsorbent, Q (L/min) is the total gas flow rate, C_0 (mg/m^3) is the inlet VOCs concentration, m (g) is the adsorbent mass, t_e (min) is the adsorption equilibrium time, C_t (mg/m^3) is the outlet VOCs concentration at any time t, t (min) is the adsorption time.

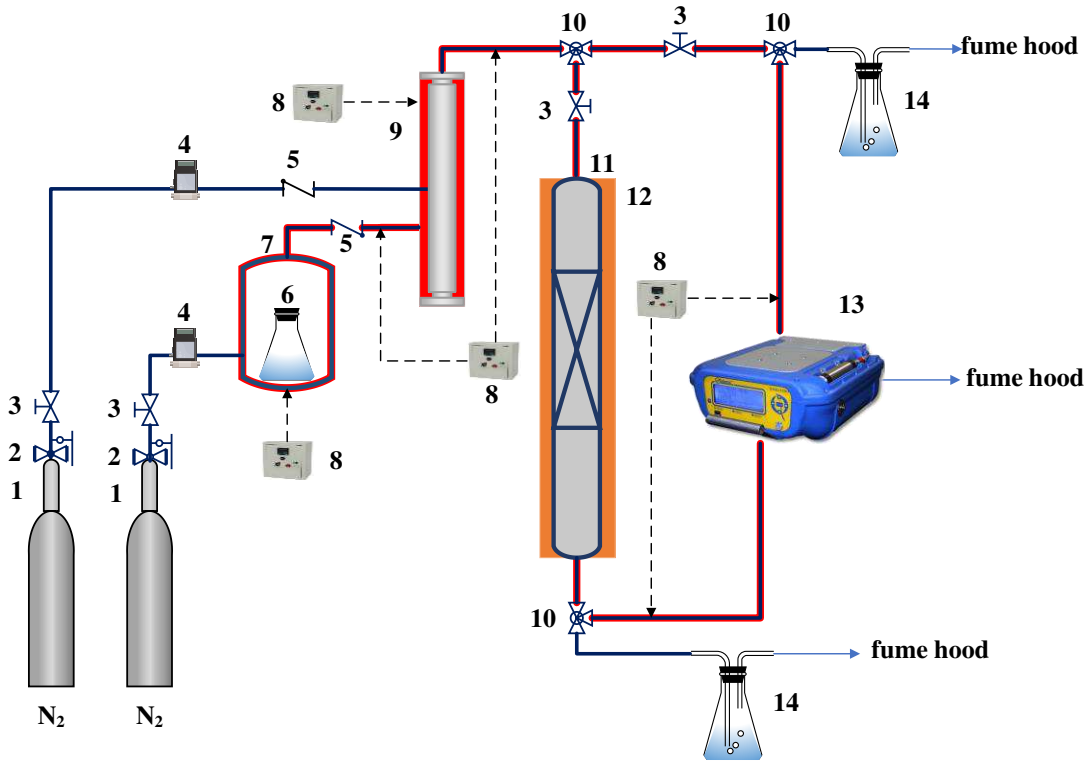

Fig.1. Schematic diagram of VOCs adsorption experimental facility. 1 High purity nitrogen tank, 2 pressure reducing valve, 3 stop valve, 4 flowmeter, 5 check valve, 6 VOCs evaporate bottle, 7 thermostat, 8 thermocouple temperature control box, 9 static mixer, 10 three-way valve, 11 quartz tube, 12 tube furnace, 13 PF300, 14 exhaust gas absorption bottle (ethyl alcohol).

2.5. Adsorption kinetic analysis

Three kinetic models were applied to analyze the adsorption behavior of VOCs on ACs, the pseudo first order model, pseudo second order model and Elovich model (Shafiei et al, 2018) respectively. The equations are as follows.

$$q_t=q_e(1-e^{-k_1t}) \quad (5)$$

$$q_t=\frac{k_2q_e^2t}{1+k_2q_et} \quad (6)$$

$$q_t=\frac{1}{\beta}\ln\alpha\beta+\frac{1}{\beta}\ln t \quad (7)$$

193 Where q_t (mg/g) and q_e (mg/g) are the adsorption capacity at time t and equilibrium, k_1
194 (min^{-1}) and k_2 ($g \cdot mg^{-1} \cdot min^{-1}$) separately represent the rate constants for the pseudo first
195 order and pseudo second order model, α ($mg \cdot g^{-1} \cdot min^{-1}$) is the initial adsorption rate
196 constant; β ($g \cdot mg^{-1}$) is the desorption rate constant.

197 Weber and Morris proposed a kinetic model for the intra particle diffusion to
198 determine rate control during adsorption (Jiang et al, 2019). The equation is as follow.

199 $$q_t = k_i t^{1/2} + C_i \quad (8)$$

200 Where k_i ($mg\ g^{-1}\ min^{-1/2}$) is the intra particle diffusion rate of adsorption process at any
201 stage, and C_i represents the intercept described the effects of boundary layer thickness.

202 **3. Results and discussion**

203 3.1. Material characterization results

204 3.1.1. Pore development and surface microstructure

205 The nitrogen adsorption-desorption isotherms and pore diameter distribution of
206 ACs are depicted in Fig. 2, specific surface area, pore volume and average pore size
207 parameters of different ACs can be seen in Table 2. For PSAC-1 and PSAC-2, the N_2
208 adsorption capacity increases rapidly in the low relative pressure region, then the
209 isotherm appears horizontal or near the surface of the horizontal platform (Fig. 2a).
210 According to the IUPAC classification, the isotherms are type I physical adsorption
211 isotherm (Ma et al., 2020), suggesting that PSAC-1 and PSAC-2 are microporous
212 materials (micro porosity: 94.41 % for PSAC-1, 92.41 % for PSAC-2). CAC nitrogen
213 adsorption-desorption isotherms belongs to type I and type IV mixture physical
214 adsorption isotherm (Gao et al., 2013). The adsorption of micropores occurs within the

range of 0 ~ 0.4 relative pressure, hysteresis loops due to capillary condensation can be observed in the range of 0.4 ~ 1.0 (Fig. 2a), this illustrates that CAC has the adsorption characteristics of mesoporous pores (microporosity: 57.55 % for CAC). PSAC-3 and PSAC-4 showed almost no adsorption of nitrogen (Fig. 2a), and PSAC-3 had only a small amount of mesoporous structure (Fig. 2b). It is not possible to perform calculations such as pore size distribution for PSAC-4 based on the isotherm data of PSAC-4 (Fig. 2a). The pore diameter distribution shows that CAC, PSAC-1 and PSAC-2 have rich pore structure (Fig. 2b). Compared with CAC, PSAC-1 and PSAC-2 have more narrow micropore structures (pore diameter < 0.7 nm), which are centrally distributed in 0.5 ~ 0.7 nm. The mesoporous structure of CAC is abundant than other two adsorption materials. The specific surface area of the four adsorbents except PSAC-4 is arranged as PSAC-3 (3.24 m^2g^{-1}) < CAC (686.76 m^2g^{-1}) < PSAC-1 (758.25 m^2g^{-1}) < PSAC-2 (1012.2 m^2g^{-1}). Therefore, AC with high specific surface area and high micropore content can be prepared from pistachio nut shell under the condition of appropriate activator.

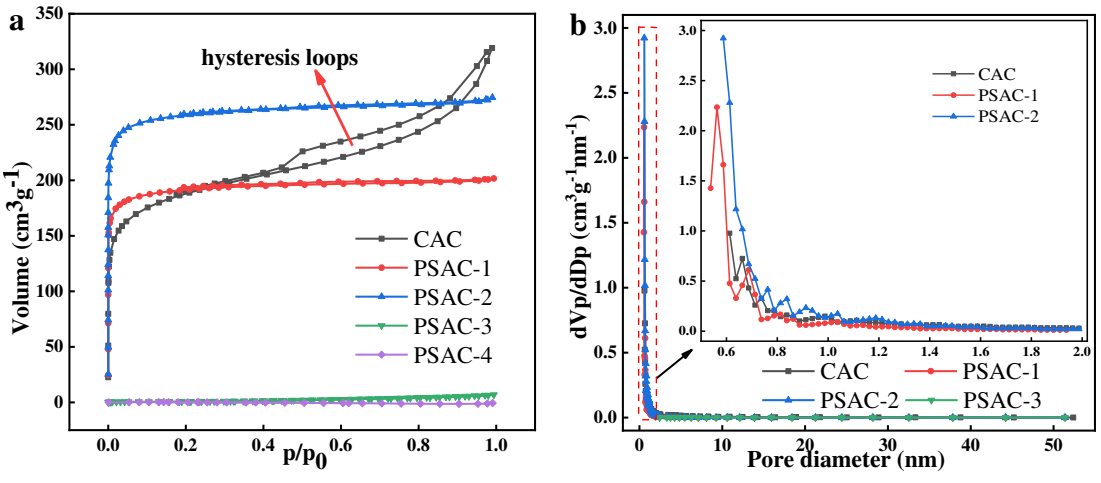

Fig. 2. N_2 adsorption-desorption isotherms of ACs (a), the pore diameter distribution and

microporous distribution magnification of ACs (b).

Table 2 - Different ACs pore parameters.

Sample	S_{BET} (m^2g^{-1})	S_{mic} (m^2g^{-1})	V_{tot} (cm^3g^{-1})	V_{mic} (cm^3g^{-1})	V_{mic}/V_{tot} (%)	D_{AC} (nm)
CAC	686.76	622.77	0.49	0.28	57.55	2.88
PSAC-1	758.25	755.22	0.31	0.29	94.41	1.64
PSAC-2	1012.2	1007.23	0.42	0.39	92.41	1.68
PSAC-3	3.24	0	0.74	0	0	12.77
PSAC-4	Cannot be calculated					

The disadvantage of the 77K N_2 adsorption method is that the diffusion kinetic energy of N_2 molecules is very low at low temperatures without sufficient diffusion into the narrow microporous pores, so the measured adsorption data are not realistic. The 273K CO_2 adsorption method can make up for the shortcomings of the 77K N_2 adsorption method to characterize the microporous pore structure.

The adsorption-desorption isotherms and characteristic curves were shown in Fig. 3. The corresponding fitting data and calculation results are shown in Table 3. The characteristic curves of the three ACs are all linear, indicating that CO_2 is mainly used to fill the micropores. The pore volume of the micropores is much larger than that measured by nitrogen adsorption, and the order of magnitude is PSAC-2 > PSAC-1 > CAC. The average pore diameter of CAC measured was still mesoporous, and PSAC-1 PSAC-2 were still microporous AC. This result was consistent with nitrogen test results, but the average pore diameter of the three kinds of carbon was significantly smaller than that measured by nitrogen adsorption, the pore size of ACs is one of the important factors affecting the adsorption process of VOCs. The characteristic curves

of PSAC-1 and PSAC-2 deviated under low pressure. The main reason was that the two ACs contained very small and narrow micropores, and CO_2 molecules could not be sufficiently diffused under low pressure, which led to this phenomenon.

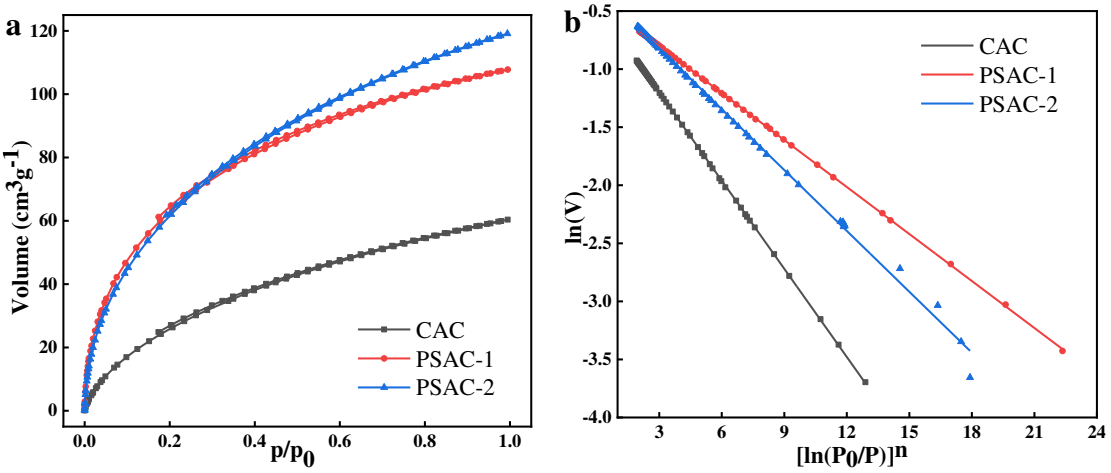

Fig. 3. CO_2 adsorption - desorption isotherm and the characteristic curve of ACS at 273K

Table 3 - Characteristic curve fitting data and ACs related parameters.

Sample	Slope	Intercept	n	R^2	V_{mic} (cm^3g^{-1})	E_0 (kJ/mol)	D_{AC} (nm)
CAC	-0.2531	-0.4416	1.51	0.9999	0.3910	16.0262	2.3345
PSAC-1	-0.1349	-0.3966	1.66	0.9999	0.4338	21.5624	1.0627
PSAC-2	-0.1747	-0.2969	1.56	0.9986	0.5457	19.7435	1.2944

Based on the adsorption test results of the above two gases, it can be concluded that the pore diameter structure of biomass AC is better than commercial coconut shell AC from every point of view. Both PSAC-1 and PSAC-2 have extremely rich micropore structure and a certain number of narrow micropores. The molecular size of most VOCs is less than 1 nm, slightly smaller than the pore diameter of PSAC-1 and PSAC-2. During the adsorption process, VOCs molecules will capillary agglomerate in the micropores to improve the adsorption amount, so PSAC-1 and PSAC-2 have a strong ability to adsorb VOCs.

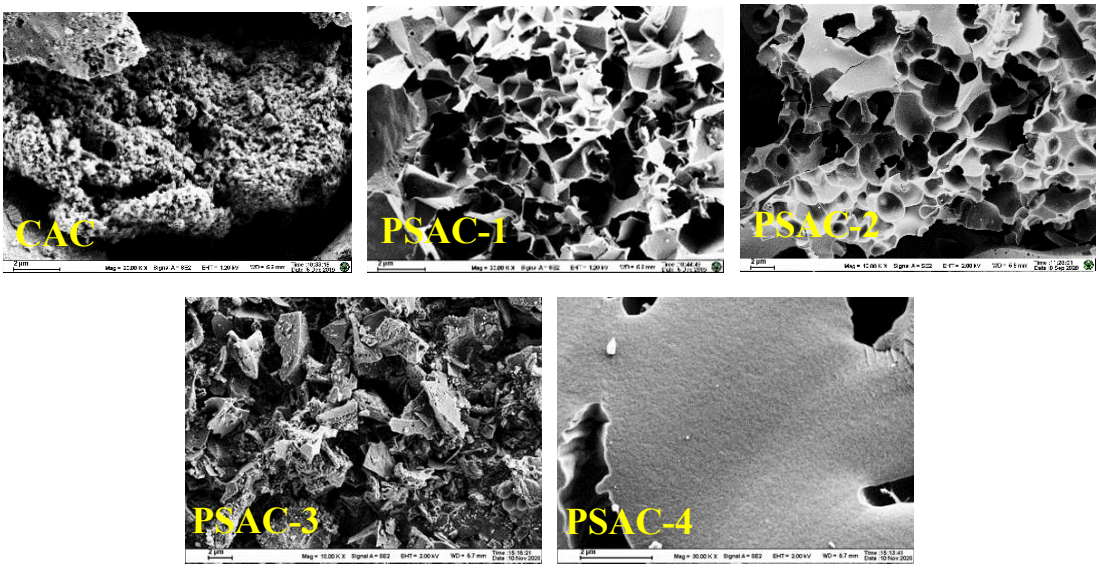

Fig. 4. The field emission scanning electron microscope images of ACs.

Fig. 4 shows surface microstructure of ACs the under the field emission scanning electron microscope, it can be seen that PSAC-1 and PSAC-2 contain rich pore structure, and the pore development is better than the commercial coconut shell AC. There are many tiny pores on the wall surface of PSAC-1 and PSAC-2, combined with its high porosity, it can be inferred that this should be the main area of adsorption. In addition, the electron microscope images of PSAC-2 showed the phenomenon of pore sleeve pore. And the surface of PSAC-3 and PSAC-4 are smooth without obvious pore structure.

3.1.2. Surface chemistry

XPS was used to analyze the chemical composition and surface functional groups of commercial coconut shell AC and biomass ACs. The corresponding results are shown in Fig. 5 and Table 4. The XPS spectra of the three ACs have three peaks, two peaks of C1s (284.7 eV) and O1s (532.4 eV) are more prominent, while those of N1s (400.5 eV) are relatively weak. The C1s peak was segmented into five peaks, which were located

at 284.6 ± 0.2 eV, 285.0 ± 0.2 eV, 286.5 ± 0.2 eV, 288.5 ± 0.2 eV and 290.4 ± 0.2 eV, respectively, corresponding to graphite carbon, C-O (connected to hydroxyl group and C in ether), C=O (C in carbonyl group), COOH (C in carboxyl group) and π-π* (Meng et al., 2019; Liu et al., 2012; Puziy et al, 2008), indicating that ACs contained some oxygen-containing functional groups. Compared with commercial AC, biomass ACs had relatively low content of π-π*, relatively high content of graphite carbon, carboxyl group and ester group, and little difference between ether, hydroxyl group and carbon group. The relative contents of the three elements (C, N, O) of PSAC-1 and PSAC-2 are similar, but the functional group contents are different. After mixed activation by adding KCl, the graphite carbon is reduced, while the ether, hydroxyl, carbon group, carboxyl group, ester group and π-π* are increased.

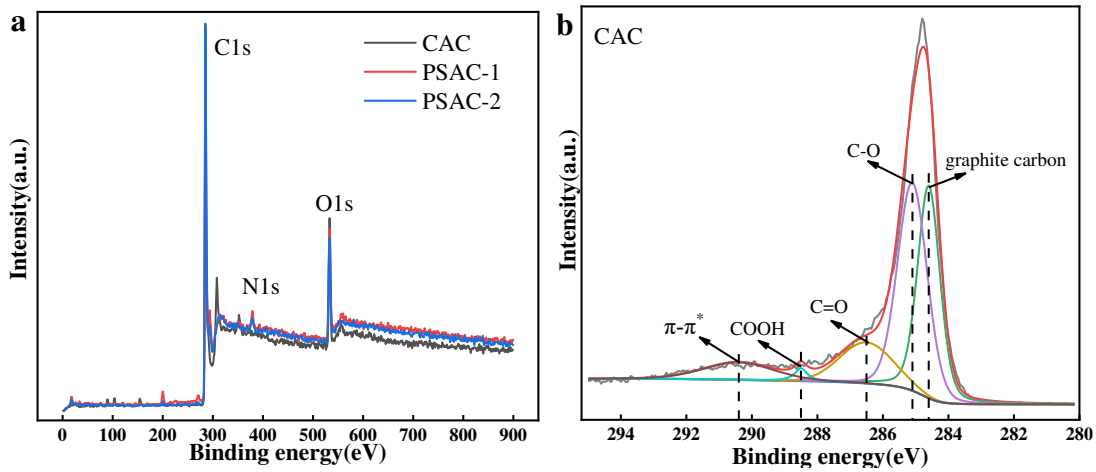

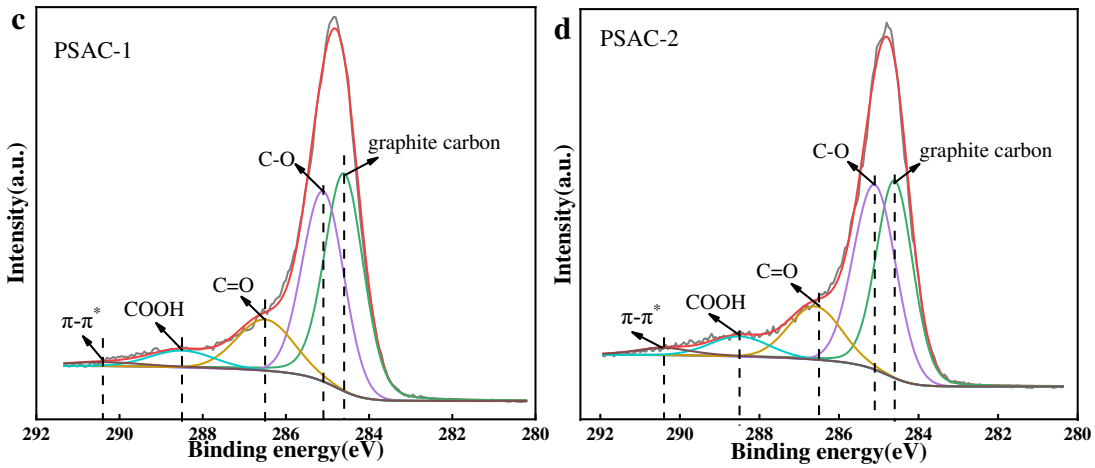

Fig. 5. The XPS spectra of survey (a), the C1s peak and the fitted curves for CAC (b), the C1s peak and the fitted curves for PSAC-1 (c), the C1s peak and the fitted curves for PSAC-2 (d).

Table 4 - Chemical compositions (wt.%) of ACs surfaces determined by XPS.

Sample	The relative content of C, N, O /%			Carbon functional group content /%				
	C	N	O	graphite carbon	C-OH/C - O-C	C=O	COOH/ COOR	π-π*
CAC	83.38	0.78	15.84	34.20	41.68	13.98	1.55	8.59
PSAC-1	83.78	0.69	15.53	42.97	36.85	13.51	4.98	1.69
PSAC-2	85.12	0.71	14.17	38.28	39.30	14.05	5.86	2.51

3.1.3. Mechanism analysis of activating agent's influence on carbonization activation

By characterization analysis of the two materials (PSAC-3, PSAC-4), it was found that the specific surface area of PSAC-3 was only units digit, while the specific surface area of PSAC-4 was too small to be calculated, and the two carbon materials had no obvious pore structure under field emission scanning electron microscope. Therefore, activation of biomass without activator or only with KCl does not have good activation

effect.

K_2CO_3 played a primary role in the activation stage. First point, K_2CO_3 reacts directly with the carbon in the biomass to increase the activation rate, as shown in the following chemical reactions Eqs (8) – (9) (Zhang et al., 2020).

$$K_2CO_3 \rightarrow K_2O + CO_2 \quad (9)$$

$$K_2O + C \rightarrow 2K + CO \quad (10)$$

Next point, under the gasification condition of C-H_2O (g), K_2CO_3 can form surface complexing salt CO^-K^+. Due to the electron-donating effect of potassium, the carbon chain breaks and disconnects, and then complexing salt is formed again, and the catalysis process of ring-opening - chain-breaking - ring-opening is repeated. In this way, at the beginning of activation, there is a condition for continuous gasification reaction near the active point containing potassium salt or potassium oxide, and gasification agent is preferred to produce macropores by successive reactions with this point and adjacent carbon.

When K_2CO_3-KCl was used for combined activation, the presence of KCl enhanced the electron-donating effect of potassium, promoted the above ring-opening - chain-breaking - ring-opening reaction process, generated the pores and expanded tiny pores. At the same time, it was also conducive to the gas passes through more biomass sites, generated holes. Therefore, the specific surface area of PSAC-2 is higher than PSAC-1, but the micro porosity is lower than PSAC-1, the phenomenon of pore sleeve pore in the SEM images of PSAC-2 can be explained (S_{BET}: 758.25 m^2g^{-1} for PSAC-1, 1012.2 m^2g^{-1} for PSAC-2, micro porosity: 94.41 % for PSAC-1, 92.41 % for PSAC-2).

3.2. Adsorption Characteristics of VOCs on ACs under low-medium temperatures

Fig. 6 shows the dynamic adsorption process of CAC, PSAC-1 and PSAC-2 at 40℃ for 5 adsorbates (benzene, toluene, p-xylene, p-dichlorobenzene and phenol) with initial concentration of 110 mg/m^3 and their corresponding saturation adsorption capacities. When the outlet concentration reaches 95% of the inlet concentration, it is considered that the adsorption reaches saturation, which is the saturation point. The dynamic adsorption process is influenced by many factors. In addition to external conditions such as adsorption temperature and initial concentration of adsorbates, the boiling point, molecular size and molecular polarity of adsorbates, pore size, specific surface area and surface functional groups of adsorbents are all important factors affecting adsorption.

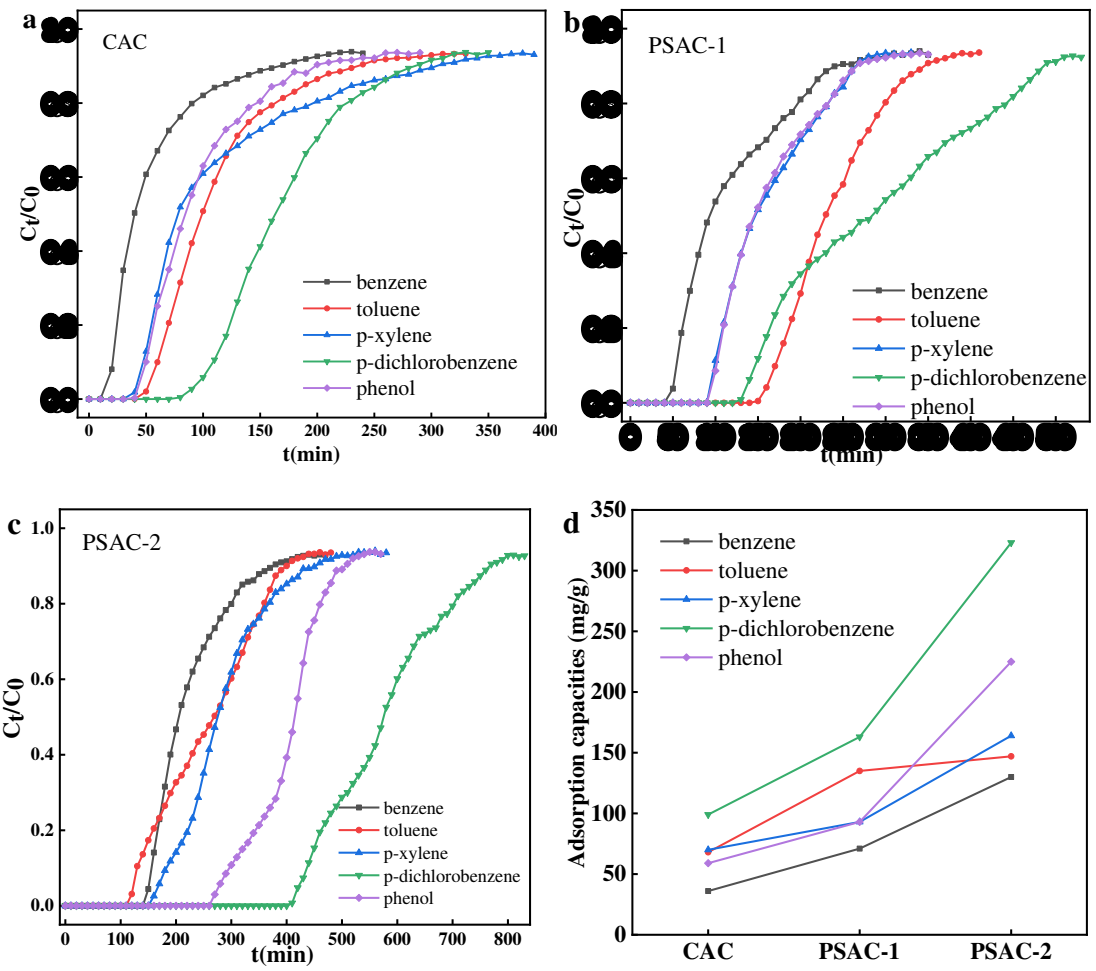

Fig. 6. Breakthrough curves of VOCs adsorption by CAC (a), breakthrough curves of VOCs adsorption by PSAC-1 (b), breakthrough curves of VOCs adsorption by PSAC-2 (c) and the corresponding adsorption capacities (d).

3.2.1. Influence of adsorbent characteristics on adsorption process

In combination with Table 2, the characterized structure of each AC and the adsorption capacity of each AC to the adsorbates, it can be seen that the larger the specific surface area is, the larger the adsorption capacity will be. Because the larger the specific surface area of AC is, the more adsorption sites it can provide for VOCs (Kim et al., 2012). Li et al. (2019) had studied that the adsorption capacity was linearly related to the specific surface area and pore volume of the adsorbent, and the linear correlation coefficient reached 0.9782 and 0.8969. This is not consistent with the experimental results in this paper, because the pore diameter distribution of ACs used in the experiment is quite different. In the process of adsorption, macropores and mesoporous usually play the role of channels, and micropores especially the narrow micropores are the main place for adsorption. Lillo-rodenas et al. (2005) found that compared with the content of micropores, the content of narrow micropores can better reflect the adsorption capacity of AC to low concentration benzene. Therefore, the adsorption capacity of VOCs on ACs is largely determined by narrow micropores. When the micropore rate is different, AC with small pore volume is also likely to absorb more VOCs. In this paper, the micropore rate of PSAC-1 and PSAC-2 is significantly higher than that of CAC, PSAC-1 and PSAC-2 are rich in narrow microporous structure. Specific surface area and VOCs adsorption capacity of PSAC-1 are all higher than CAC,

but the pore volume of CAC is larger than PSAC-1, this is because the micropore volume of PSAC-1 is higher than CAC. Therefore, the adsorption effect should not only consider the total pore volume, but also the micropore volume, there isn't a good linear relationship between pore volume and adsorption capacity in our research.

3.2.2. Influence of adsorbate characteristics on adsorption process

Three adsorbates with the same intramolecular element composition: benzene (80.1℃), toluene (110.6℃) and paraxylene (138.5℃) are selected for discussion here. Apart from the adsorption of PSAC-1 to p-xylene, the adsorption capacity increased with the increase of the boiling point of the adsorbates,. Chiang et al. (2001) and Guo et al. (2012) had found that VOC adsorption on porous adsorbents is similar to the process of vapor-liquid phase transformation and liquid-like condensation, that is, the adsorbate changes from gas phase to liquid phase in the adsorbent pores. VOCs with high boiling point are preferentially adsorbed because they are easier to be converted into liquid and have stronger intermolecular forces with adsorbents. It was also observed that CAC and PSAC-2 had no obvious increase in p-xylene adsorption, because in addition to the effect of the boiling point of the adsorbent on the adsorption process, the molecular size of the adsorbate also affected the adsorption process. In the same situation, the VOCs molecule size is larger than the pore diameter, no adsorption occurs due to steric hindrance, the VOCs molecule size is equal to the pore diameter, which has strong biochar trapping power and is not easy to desorption. The VOCs molecule size is smaller than the pore diameter, and the capillary condensation phenomenon occurs in the pore, which makes the biochar adsorption capacity large.

The VOCs molecule size is much smaller than the pore diameter, and the adsorption molecules are easy to desorption, which leads to a decrease in the capacity of adsorption (Li et al., 2019). The three ACs used in our experiment were all contain narrow micropores. Compared with CAC and PSAC-2, PSAC-1 has a higher content of narrow micropores and a wider distribution, with the narrowest pore diameter up to less than 0.6 nm. As shown in Table 1, the molecular size of p-xylene is larger than benzene and toluene. Therefore, when the difference between the boiling point and molecular weight of VOCs is less, it may be that the molecular size of p-xylene is larger than the pore diameter of ACs, resulting in a decrease or insignificant increase in its adsorption.

It can be observed from Fig. 6 that the adsorption capacity of p-dichlorobenzene is larger than that of benzene, toluene and p-xylene with smaller molecular size, this is because the boiling point of p-dichlorobenzene is nearly 40℃ higher than benzene, toluene and p-xylene, and the molecular weight difference exceeds 40, the difference of boiling point and molecular weight leads to the more easy conversion of p-dichlorobenzene in the adsorbent hole and the increase of liquid phase condensation adsorption. Such a rule can also explain that the adsorption capacity of toluene and p-xylene is higher than that of benzene. Meanwhile, the abundant oxygen-containing functional groups on the surface of AC can increase the dipole-dipole interaction between AC and p-dichlorobenzene, promote adsorption (Almazán-Almazán et al., 2007), and increase the adsorption capacity. It was found that the adsorption capacity of ACs for dichlorobenzene was greater than that of phenol, which has a higher boiling point and smaller molecular size. This is because phenol molecules contain hydroxyl

groups and are more polar than the other four VOCs, while the surface of ACs is dominated by non-polar C-C. The adsorption capacity of ACs for polar molecules is much weaker than that of non-polar molecules.

3.3. Influence of temperature on adsorption

Temperature is one of the important external factors affecting adsorption, Fig. 7 shows the dynamic adsorption process and saturation adsorption capacities of toluene with initial concentration of 110 mg/m^3 for CAC, PSAC-1 and PSAC-2 at 40 ºC, 55 ºC and 70 ºC, respectively. Obviously, it can be concluded from Fig. 7 that in the temperature range of medium and low temperature, with the increase of adsorption temperature, the adsorption capacity of AC to toluene gas decreases, and the diffusion time is shortened. This is because the adsorption process of AC on VOCs is dominated by physical adsorption, which is an exothermic process. When the temperature rises, the adsorption process will be inhibited and the reversible process will proceed towards desorption. As the temperature rises, the kinetic energy of VOCs molecules increases, which accelerates the diffusion rate of molecules through macropores and mesoporous, so the penetration time decreases. By comparing the penetration curves of PSAC-1, PSAC-2 and CAC, it was found that when the temperature rose from 55 to 70 ºC, the adsorption process of CAC was not distinct affected, and the corresponding adsorption capacity was not visible reduced as compared with that of PSAC-1 and PSAC-2. The reasons can be analyzed from two aspects, in the one aspect, temperature have bigger influence on the adsorption process of micro pores, suppresses the condensation process of the gaseous toluene inside the micropores. Compared with PSAC-1 and PSAC-2, the

microporous content of CAC is less, while the mesoporous content of CAC is more, toluene molecules already had a fast diffusion rate between CAC pores under the low temperature. In the other aspect, a rise in temperature will lead to an increase in chemical adsorption. Compared with PSAC-1 and PSAC-2, CAC has fewer acidic oxygen-containing functional groups. With the decrease of acidic oxygen-containing groups on AC surface, the polarity of AC surface decreased, the chemical adsorption of weakly polar toluene by CAC is stronger than that of PSAC-1 and PSAC-2. Therefore, the temperature affected less on the CAC adsorption process.

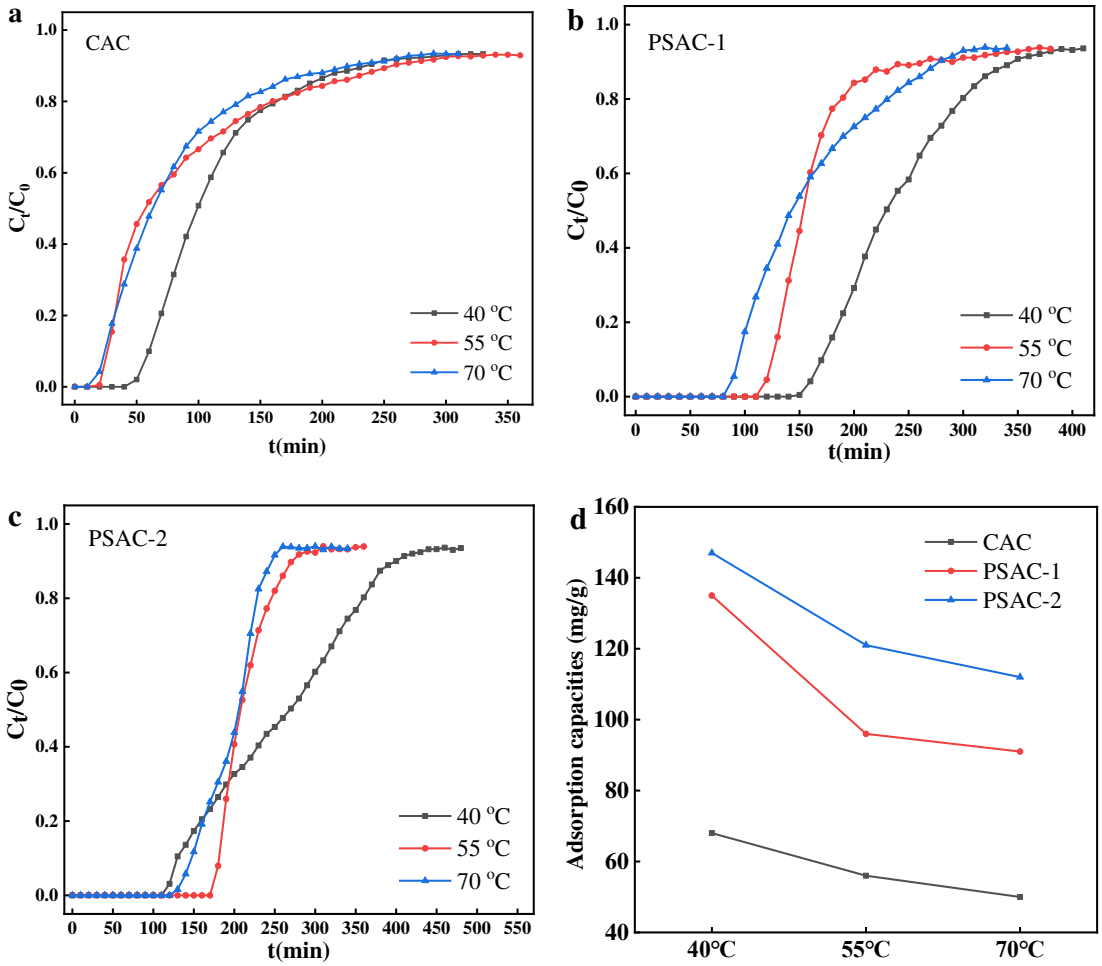

Fig. 7. Breakthrough curves of toluene adsorption by CAC under different temperature (a), breakthrough curves of toluene adsorption by PSAC-1 under different temperature (b),

breakthrough curves of toluene adsorption by PSAC-2 under different temperature (c) and the corresponding adsorption capacities (d).

3.4. Adsorption Kinetics Analysis

3.4.1. Kinetics Model Fitting

From the above experimental data, the adsorption processes of two VOCs (toluene and p-dichlorobenzene) with large differences in molecular weight and boiling point on micro mesoporous AC (CAC) and microporous AC (PSAC-2) were selected for kinetic model fitting, respectively, as shown in Fig. 8, the corresponding calculated results are shown in Table 5. According to the calculation results, pseudo first-order kinetic model fitting results were better, R_2 (0.9894~0.9965) was greater than the other two models, and the fitted equilibrium adsorption amount was more in line with the experimental value. According to the pseudo first-order kinetic model's assumption (Drenkova-Tuhtan et al., 2017), it can be concluded that the adsorption velocity was determined by the diffusion step of the adsorption process, and the adsorption rate is positively correlated with the adsorption capacity at equilibrium and the adsorption capacity difference at a certain time point. It can be found from Table 5 that the rate constant (k_1) of PSAC-2 is lower than that of CAC, which is caused by the richer mesoporous content of CAC and the faster diffusion rate of VOCs in it. So, a certain number of mesopores helps to accelerate the adsorption rate. The rate constant (k_1) of p-dichlorobenzene is lower than that of toluene, due to the higher molecular weight and boiling point of p-dichlorobenzene, resulting in a lower molecular diffusion rate. Pseudo second-order kinetic model for adsorption of VOCs can also do it better fitting and R_2 value can reach

0.9826~0.9892, Elovich model except for p-dichlorobenzene in adsorption process of PSAC-2 on the fitting result is poorer, R_2 value can reach 0.9447~0.9831, this indicates that the adsorption process is also affected by certain chemical adsorption (Zhang et al., 2019), which is related to the part of oxygen-containing functional groups on the surface of ACs.

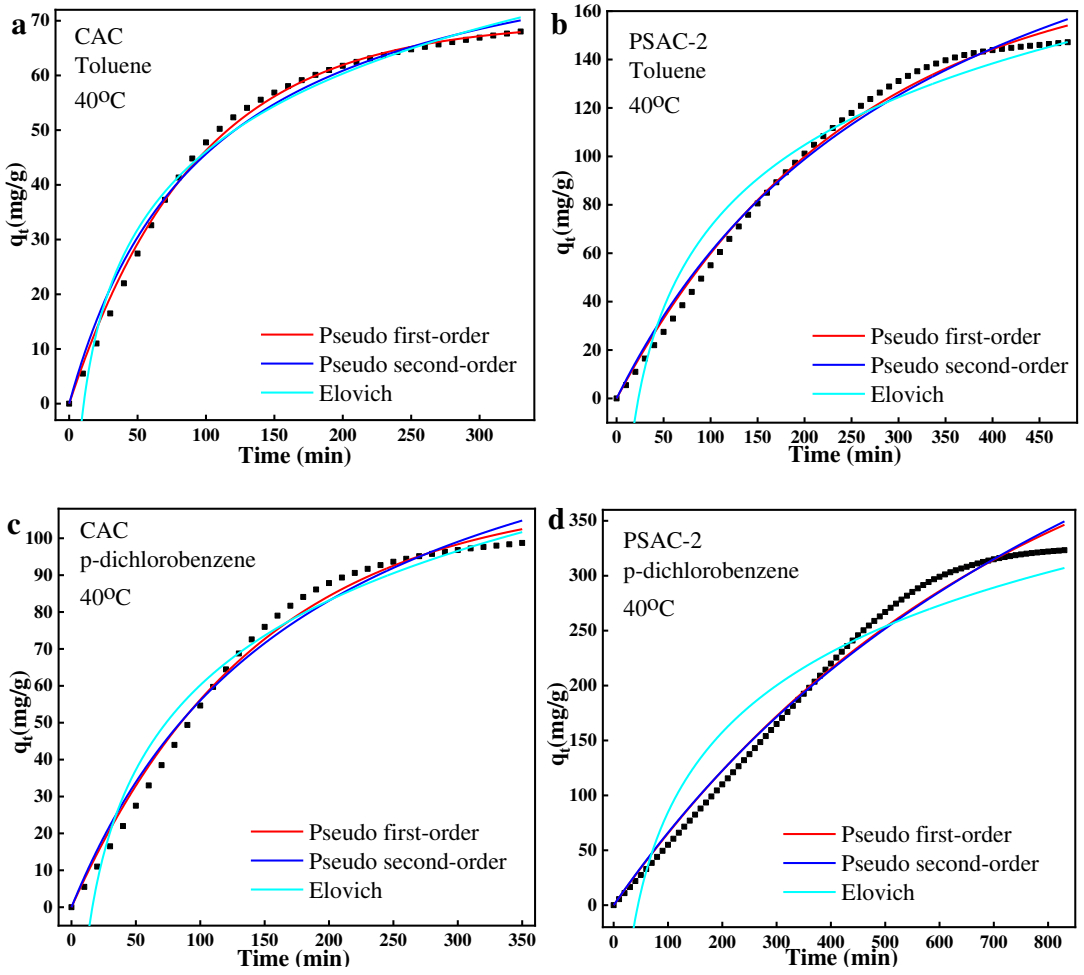

Fig. 8. Nonlinear fitting curves of three kinetic models. Fitting curves of toluene adsorption process by CAC (a). Fitting curves of toluene adsorption process by PSAC-1 (b). Fitting curves of p-dichlorobenzene adsorption process by CAC (c). Fitting curves of p-dichlorobenzene adsorption process by PSAC-1 (d).

Table 5 - Kinetic parameters of toluene and p-dichlorobenzene adsorption by ACs.

kinetic models and parameters	Toluene		P-dichlorobenzene	
	CAC	PSAC-2	CAC	PSAC-2

Pseudo first-order	q_e (mg/g)	69.8583	179.7455	112.3763	508.3224
	k_1 (min^{-1})	0.0109	0.0041	0.0069	0.0014
	R^2	0.9965	0.9932	0.9897	0.9894
Pseudo second-order	q_e (mg/g)	91.3081	269.2277	160.8911	848.2437
	k_2 ($g \cdot mg^{-1} \cdot min^{-1}$)	0.00011	0.00001	0.00003	0.000001
	R^2	0.9887	0.9892	0.9826	0.9877
Elovich	α ($mg \cdot g^{-1} \cdot min^{-1}$)	1.9302	2.1026	2.0388	2.3556
	β ($g \cdot mg^{-1}$)	0.0487	0.0205	0.0302	0.0095
	R^2	0.9831	0.9447	0.9624	0.8853

3.4.2. Rate-controlling Mechanism

In order to further determine the mechanism of adsorption, the Weber-Morris kinetic model was used to simulate it. The fitting results are shown in Fig. 9, none of the straight line cross through the origin, indicating that intra particle diffusion is not the only mechanism to control the adsorption rate, combined with the above adsorption kinetic analysis, this phenomenon may be caused by the presence of chemical adsorption in the adsorption process, which accelerates the adsorption rate. Three stages (Jiang et al., 2019) adsorption rate constants were obtained and listed in Table 6. The VOCs adsorption process can be explain according to the above analysis, (A) VOCs molecules diffuse from the gas phase to the surface of AC, which is mainly affected by the outer surface area of AC and initial concentration of VOCs. The flat curve of stage in Fig. 9 corresponds to the small value of k_A in Table 6, and the VOCs concentration in this experiment is low, so this stage controls the adsorption process rate. (B) VOCs molecules adsorbed on the surface of AC diffused into the internal structure of AC through the pores of AC, and the diffusion rate depends on the pore diameter

distribution of AC. It can be seen from Fig. 9 and Table 6 that the diffusion rate at this stage is faster than the last stage, So, the more micropores, the faster the diffusion rate. (C) With the increase of VOCs molecules entering the AC, the free channel of VOCs molecules becomes narrower, the diffusion process is blocked, in Fig. 9 the curve of this stage flattens again, the adsorption process slows down, and finally the adsorption reaches equilibrium.

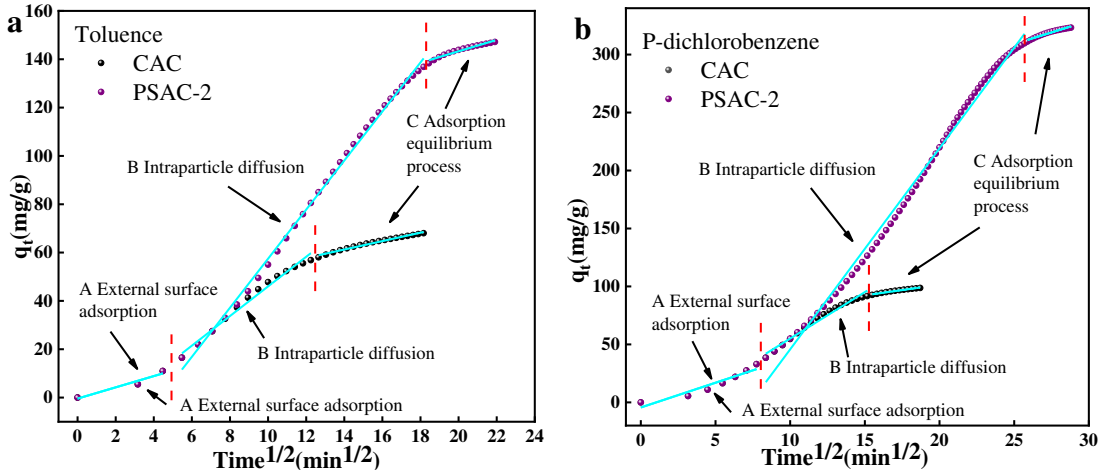

Fig. 9. Intraparticle diffusion kinetic plots for toluene and p-dichlorobenzene adsorption. Fitting of toluene adsorption processes at CAC and PSAC-1, respectively (a). Fitting of p-dichlorobenzene adsorption processes at CAC and PSAC-1, respectively (b).

Table 6 - The fitting constant values of Weber-Morris kinetic model.

Kinetic parameters		Toluene		P-dichlorobenzene	
		CAC	PSAC-2	CAC	PSAC-2
External surface adsorption	k_A (mg g^{-1} $min^{-1/2}$)	2.3266	2.3266	4.2700	4.2700
	C_A	-0.4028	-0.4208	-4.3941	-4.3941
	R^2	0,8918	0.8919	0.8949	0.8949
Intraparticle diffusion	k_B (mg g^{-1} $min^{-1/2}$)	6.1292	10.1493	8.0095	17.3441
	C_B	-15.2888	-44.0191	-25.0251	-127.6827
	R^2	0.9841	0.9973	0.9776	0.9932

Adsorption	k_C (mg g^{-1} $min^{-1/2}$)	1.7427	2.3582	1.8167	4.0090
equilibrium	C_C	36.8670	96.1243	65.0770	208.8316
process	R^2	0.9838	0.9536	0.9798	0.9615

4. Conclusions

AC of pistachio shell with high specific surface area and micro porosity can be prepared by using K_2CO_3 and KCl to activate the shell. Rich micropore structure and a certain number of narrow micropore making biomass ACs have a strong ability to adsorb VOCs. The performance of biomass ACs is better than that of commercial coconut shell AC, among which the AC prepared by combined activation has the best performance.

Microporous pistachio shell AC has excellent adsorption performance for low concentration VOCs at low-medium temperature. The adsorption capacity of toluene and p-dichlorobenzene is up to 147 mg/g and 323 mg/g. Its maximum adsorption capacity can reach 3.8 times of the commercial AC adsorption capacity. From the perspective of ACs, the larger the specific surface area and micropore volume are, the larger the adsorption capacity will be. From the perspective of VOCs, the higher the boiling point, the greater the molecular weight and the weaker the molecular polarity are conducive to adsorption on activated carbon. When the molecular size of VOCs is slightly smaller than the pore size of activated carbon, its adsorption capacity increases.

In the temperature range of low and medium temperature, with the increase of adsorption temperature, the adsorption capacity of ACs to toluene gas decreases, and the penetration time is shortened. The increase of temperature will increase chemical adsorption and affect the adsorption process of AC with high micropores content.

All the three adsorption kinetic models can have a good fitting curve for the adsorption process. The adsorption process of biomass activated carbon on VOCs is dominated by physical adsorption, while there is also a certain amount of chemical adsorption. There are three stages in the process of VOCs adsorption, due to the low VOCs concentration, the first stage of external membrane mass transfer is the control stage of adsorption rate.

Ethical Approval

Not applicable

Consent to Participate

Not applicable

Consent to Publish

Not applicable

Authors Contributions

Tangying Cheng: Conceptualization, Methodology, Formal analysis, Investigation, Resources, Writing - Original Draft, Writing - Review & Editing.

Jinjin Li: Methodology, Investigation, Writing - Review & Editing.

Xiuwei Ma: Methodology, Resources, Writing - Review & Editing.

Lei Zhou and Hao Wu: Conceptualization, Writing - Review & Editing, Supervision.

Linjun Yang: Conceptualization, Writing - Review & Editing, Supervision, Project administration, Funding acquisition.

Funding

Funding is acknowledged from the National Key Research and Development Program of China (2018YFB0605200).

Competing Interests

The authors declare that they have no competing interests.

Availability of data and materials

All data generated or analysed during this study are included in this published article and its supplementary information files.

References

Açıkalın, K., Karaca, F., Bolat, E., 2012. Pyrolysis of pistachio shell: effects of pyrolysis conditions and analysis of products. Fuel 95, 169–177.

Almazán-Almazán, M.C., Pérez-Mendoza, M., Domingo-García, M., Fernández-Morales, I., Rey-Bueno, F.D., García-Rodríguez, A., López-Garzón, F.J., 2007. The role of the porosity and oxygen groups on the adsorption of n-alkanes, benzene, trichloroethylene and 1,2-dichloroethane on active carbons at zero surface coverage. Carbon. 45, 1777-1785.

Bazan-Wozniak, A., Nowicki, P., Pietrzak, R., 2017. The influence of activation procedure on the physicochemical and sorption properties of activated carbons prepared from pistachio nutshells for removal of NO_2/H_2S gases and dyes. J. Clean Prod. 152, 211-222.

Cardoso, B., Mestre, A.S., Carvalho, A.P., Pires, J., 2008. Activated Carbon Derived from Cork Powder Waste by KOH Activation: Preparation, Characterization, and VOCs Adsorption. Ind. Eng. Chem. Res. 47, 5841–5846.

Cazorla-Amorós, D., Alcañiz-Monge, J., de la Casa-Lillo, M. A., Linares-Solano, A., 1998. CO_2 As an Adsorptive To Characterize Carbon Molecular Sieves and Activated Carbons. Langmuir. 14, 4589-4596.

Cheng, J., Zhang, Y.S., Wang, T., Xu, H., Norris, P., Pan, W.P., 2018. Emission of volatile organic compounds (VOCs) during coal combustion at different heating rates. Fuel. 225, 554-562.

Chiang, Y.C., Chiang, P.C., Huang, C.P., 2001. Effects of pore structure and temperature

on VOC adsorption on activated carbon. Carbon. 39, 523-534.

Deng, S., Nie, Y., Du, Z.W., Huang, Q., Meng, P.P., Wang, B., Huang, J., Yu, G, 2015. Enhanced adsorption of perfluorooctane sulfonate and perfluorooctanoate by bamboo-derived granular activated carbon. J. Hazard. Mater. 282, 150-157.

Dolas, H., Sahin, O., Saka, C., Demir, H., 2011. A new method on producing high surface area activated carbon: The effect of salt on the surface area and the pore size distribution of activated carbon prepared from pistachio shell. Chem. Eng. J. 166, 191-197.

Drenkova-Tuhtan, A., Schneider, M., Franzreb, M., Meyer, C., Gellermann, C., Sextl, G., Mandel, K., Steinmetz, H., 2017. Pilot-scale removal and recovery of dissolved phosphate from secondary wastewater effluents with reusable ZnFeZr adsorbent @ Fe_3O_4/SiO_2 particles with magnetic harvesting. Water Res. 109, 77-87.

Foo, K.Y., Hameed, B.H., 2011. Preparation and characterization of activated carbon from pistachio nut shells via microwave-induced chemical activation. Biomass Bioenerg. 35, 3257-3261.

Foroushani, F.T., Tavanai, H., Hosseini, F.A., 2016. An investigation on the effect of $KMnO_4$ on the pore characteristics of pistachio nut shell based activated carbon. Microporous Mesoporous Mat. 230, 39-48.

Gao, Y., Yue, Q.Y., Gao, B.Y., Sun, Y.Y., Wang, W.Y., Li, Q., Wang, Y., 2013. Comparisons of porous, surface chemistry and adsorption properties of carbon derived from Enteromorpha prolifera activated by $H_4P_2O_7$ and KOH. Chem. Eng. J. 232, 582-590.

590 Guo, Y.Y., Li, Y., Zhu, T.Y., Ye, M., 2012. Effects of Concentration and Adsorption
591 Product on the Adsorption of SO_2 and NO on Activated Carbon. Energy Fuels. 27,
592 360-366.
593 Jiang, S.B., Yu, T.F., Xia, R., Wang, X., Gao, M.Z., 2019. Realization of super high
594 adsorption capability of 2D δ-MnO_2 /GO through intra-particle diffusion. Mater.
595 Chem. Phys. 232, 374-381.
596 Hadoun, H., Sadaoui, Z., Souami, N., 2013. Characterization of mesoporous carbon
597 prepared from date stems by H_3PO_4 chemical activation. Appl. Surf. Sci., 280, 1-7.
598 Kaghazchi, T., Kolur, N. A., Soleimani, M., 2010. Licorice residue and Pistachio-nut
599 shell mixture: A promising precursor for activated carbon. J. Ind. Eng. Chem. 16,
600 368-374.
601 Kamandari, H., Hashemipour, H., Najjarzadeh, H., Eksiri, Z., 2015. Influence of
602 process variables on chemically activated carbon from pistachio shell with $ZnCl_2$
603 and KOH. Res. Chem. Intermed. 41, 71-81.
604 Kamandari, H., Hashemipour, H., Saeednia, L.,2013. Experimental and modeling study
605 on production of activated carbon from pistachio shells in rotary reactor. Res. Chem.
606 Intermed. 40, 509-521.
607 Kim, K.J., Ahn, H.G., 2012. The effect of pore structure of zeolite on the adsorption of
608 VOCs and their desorption properties by microwave heating. Microporous
609 Mesoporous Mat. 152, 78-83.
610 Li, X.Q., Zhang, L., Yang, Z.Q., Wang, P., Yan, Y.F., Ran, J.Y., 2020. Adsorption
611 materials for volatile organic compounds (VOCs) and the key factors for VOCs

adsorption process: A review. Sep. Purif. Technol. 235, 116213.

Lillo-Ródenas, M.A., CazorlHa-Amorós, D., Linares-Solano, A., 2005. Behaviour of activated carbons with different pore size distributions and surface oxygen groups for benzene and toluene adsorption at low concentrations. Carbon. 43, 1758-1767.

Liu, J., Wang, J.W., Cheng, J., Zhang, Y.S., Wang, T., Pan, W.P., 2020. Distribution and emission of speciated volatile organic compounds from a coal-fired power plant with ultra-low emission technologies. J. Clean Prod. 264, 121686.

Liu, Y., Guo, Y.P., Gao W., Wang, Z., Ma Y.J, Wang, Z.C., 2012. Simultaneous preparation of silica and activated carbon from rice husk ash. J. Clean Prod. 32, 204-209.

Liu, Z.H., Qiu, J.R., Liu, H., Tan, Z.Q., Yan, Z.Q., Zhang, M.L., Zeng, H.C., Yang, H., 2012. Effects of SO_2 and NO on removal of VOCs from simulated flue gas by using activated carbon fibers at low temperatures. Journal of Fuel Chemistry & Technology. 40, 93-99.

Lua, A.C., Yang, T., 2004a. Properties of pistachio-nut-shell activated carbons subjected to vacuum pyrolysis conditions. Carbon. 42, 224-226.

Lua, A.C., Yang, T., 2004c. Effect of activation temperature on the textural and chemical properties of potassium hydroxide activated carbon prepared from pistachio-nut shell. J. Colloid Interface Sci. 274, 594-601.

Lua, A.C., Yang, T., 2004d. Effects of vacuum pyrolysis conditions on the characteristics of activated carbons derived from pistachio-nut shells. J. Colloid Interface Sci. 276, 364-372.

Lua, A.C., Yang, T., 2005. Characteristics of activated carbon prepared from pistachio-nut shell by zinc chloride activation under nitrogen and vacuum conditions. J. Colloid Interface Sci. 290, 505-513.

Lua, A.C., Yang, T., Guo, J., 2004b. Effects of pyrolysis conditions on the properties of activated carbons prepared from pistachio-nut shells. J. Anal. Appl. Pyrolysis. 72, 279-287.

Ma, X.W., Zhang, Z., Wu, H., Li, J.J., Yang, L.J., 2020. Adsorption of Volatile Organic Compounds at Medium High Temperature Conditions by Activated Carbons. Energy Fuels. 34, 3679-3690.

Marett, J., Aning, A., Foster, E. J., 2017. The isolation of cellulose nanocrystals from pistachio shells via acid hydrolysis. Ind. Crop. Prod. 109, 869-874.

Meng, F.Y., Song, M, Wei, Y.X., Wang, Y.L., 2019. The contribution of oxygen-containing functional groups to the gas-phase adsorption of volatile organic compounds with different polarities onto lignin-derived activated carbon fibers. Environ. Sci. Pollut. Res. 26, 7195-7204.

Niksiar, A., Nasernejad, B., 2017. Activated carbon preparation from pistachio shell pyrolysis and gasification in a spouted bed reactor. Biomass Bioenerg. 106, 43-50.

Niksiar, A., Nasernejad, B., 2018. Modeling of gasification reaction to produce activated carbon from pistachio shells in a spouted bed. Biomass Bioenerg. 119, 97-108.

Puziy, A.M., Poddubnaya, O.I., Socha, R.P., Gurgul, J., Wisniewski, M., 2008. XPS and NMR studies of phosphoric acid activated carbons. Carbon, 46, 2113-2123.

656 Qu, F., Zhu, L.Z., Yang, K., 2009. Yang Adsorption behaviors of volatile organic
657 compounds (VOCs) on porous clay heterostructures (PCH). J. Hazard. Mater. 170,
658 7-12.
659 Sarswata, A., Mohan, D., 2016. Sustainable development of coconut shell activated
660 carbon (CSAC) & magnetic coconut shell activated carbon (MCSAC) for phenol
661 (2-nitrophenol) removal. Rsc Adv, 6, 85390.
662 Shafiei, M., Alivand, M.S., Rashidi, A., Samimi, A., Mohebbi-Kalhori, D., 2018.
663 Synthesis and adsorption performance of a modified micro-mesoporous MIL-
664 101(Cr) for VOCs removal at ambient conditions. Chem. Eng. J. 341, 164-174.
665 Song, M.D., Liu, X.A., Zhang, Y.H., Shao, M., Lu, K.D., Tan, Q.W., Feng, M., Qu, Y.,
666 2019. Sources and abatement mechanisms of VOCs in southern China. Atmos.
667 Environ. 201, 28-40.
668 Vijayalakshmi, P., Bala, V.S.S., Thiruvengadaravi, K.V., Panneerselvam, P.,
669 Palanichamy, M., Sivanesan, S., 2010. Removal of Acid Violet 17 from Aqueous
670 Solutions by Adsorption onto Activated Carbon Prepared from Pistachio Nut Shell.
671 Sep. Sci. Technol. 46, 155-163.
672 Yang, K., Yang, J.T., Jiang, Y., Wu, W.H., Lin, D.H., 2016. Correlations and adsorption
673 mechanisms of aromatic compounds on a high heat temperature treated bamboo
674 biochar. Environ. Pollut. 210, 57-64.
675 Yang, T., Lua, A.C., 2003. Characteristics of activated carbons prepared from pistachio-
676 nut shells by physical activation. J. Colloid Interface Sci. 267, 408-417.
677 Yang, T., Lua, A.C., 2006. Textural and chemical properties of zinc chloride activated

678 carbons prepared from pistachio-nut shells. Mater. Chem. Phys. 100, 438-444.
679 Zhang, B.P., Yang, D.J., Qiu, X.Q., Qian, Y., Yan, M.Z., Li, Q., 2020. Influences of
680 aggregation behavior of lignin on the microstructure and adsorptive properties of
681 lignin-derived porous carbons by potassium compound activation. J. Ind. Eng.
682 Chem. 82, 220-227.
683 Zhang, G.X., Liu, Y.Y., Zheng, S.L., Hashisho, Z., 2019. Adsorption of volatile organic
684 compounds onto natural porous minerals. J. Hazard. Mater. 364, 317–324.

Figures

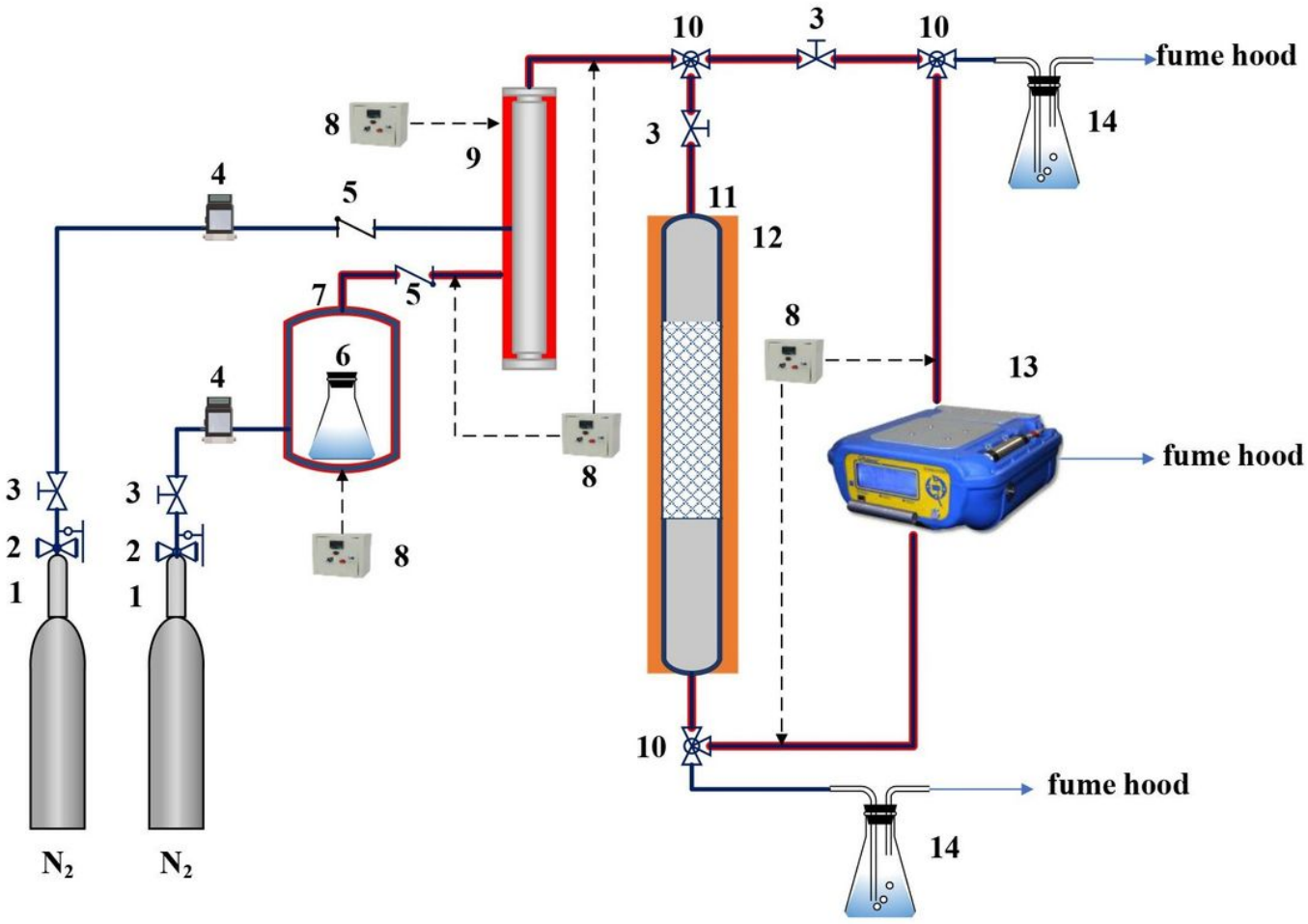

Figure 1

Schematic diagram of VOCs adsorption experimental facility. 1 High purity nitrogen tank, 2 pressure reducing valve, 3 stop valve, 4 flowmeter, 5 check valve, 6 VOCs evaporate bottle, 7 thermostat, 8 thermocouple temperature control box, 9 static mixer, 10 three-way valve, 11 quartz tube, 12 tube furnace, 13 PF300, 14 exhaust gas absorption bottle (ethyl alcohol).

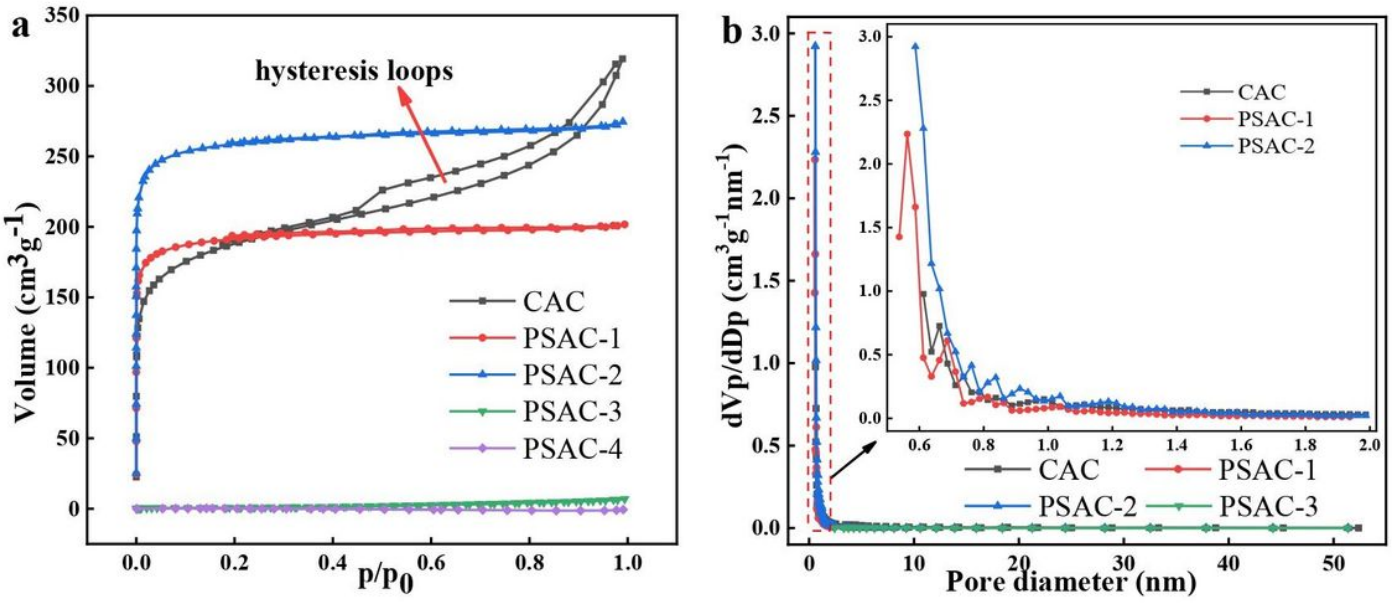

Figure 2

N2 adsorption-desorption isotherms of ACs (a), the pore diameter distribution and microporous distribution magnification of ACs (b).

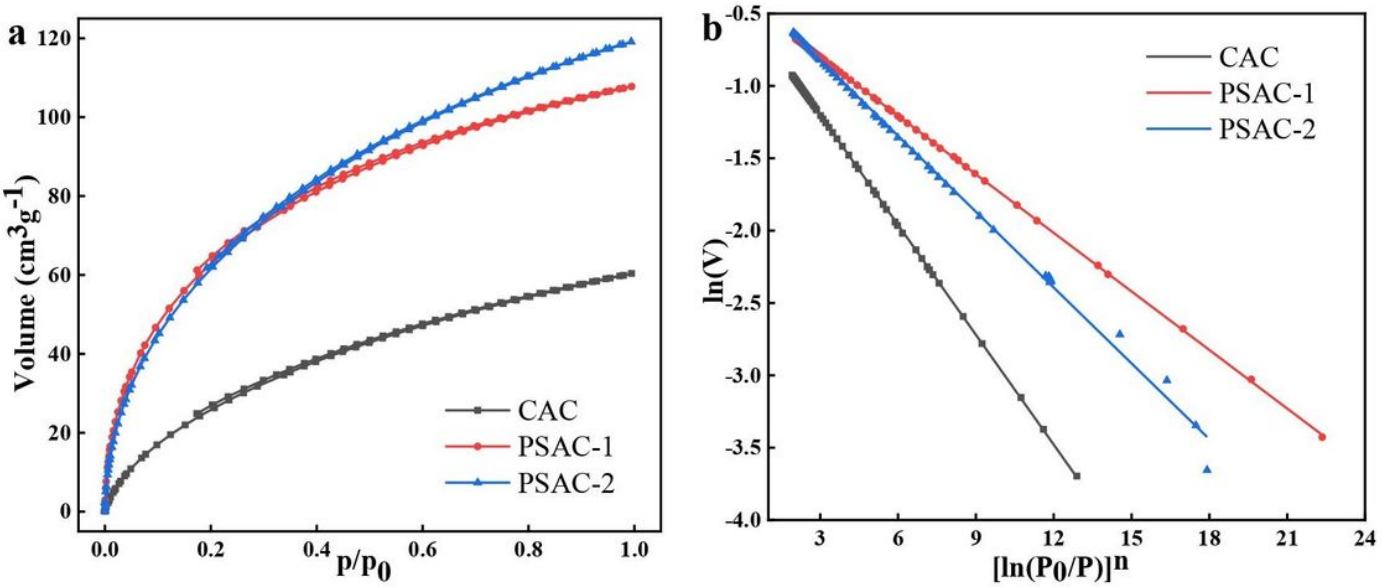

Figure 3

CO2 adsorption - desorption isotherm and the characteristic curve of ACS at 273K

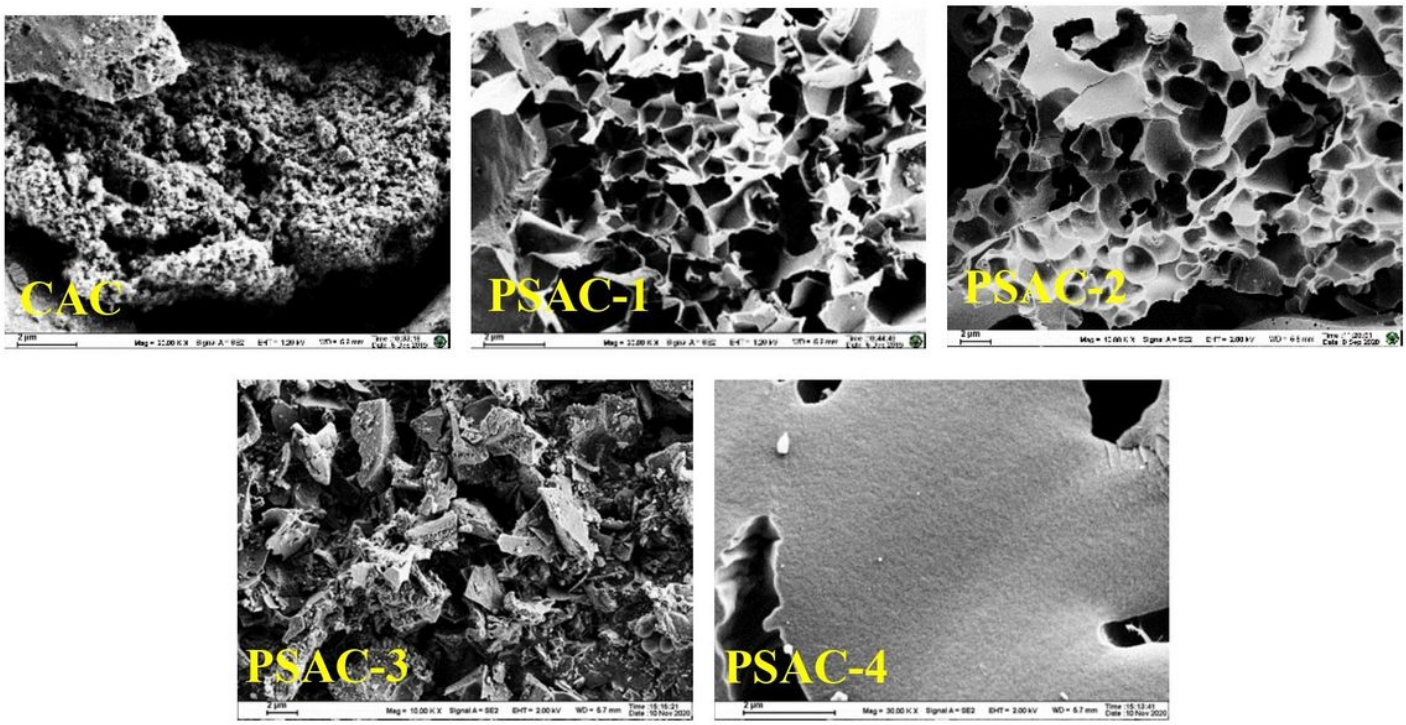

Figure 4

The field emission scanning electron microscope images of ACs.

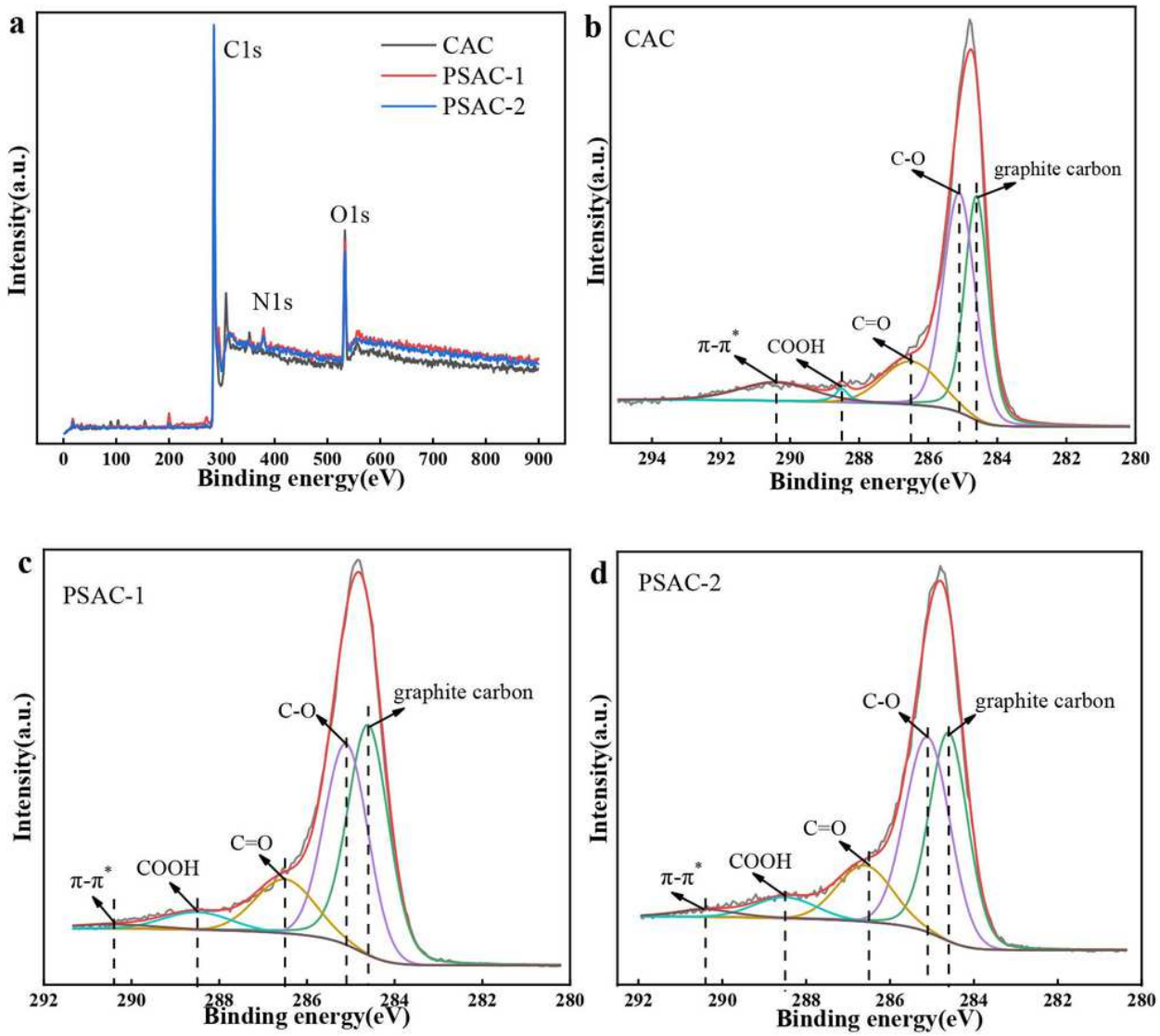

Figure 5

The XPS spectra of survey (a), the C1s peak and the fitted curves for CAC (b), the C1s peak and the fitted curves for PSAC-1 (c), the C1s peak and the fitted curves for PSAC-2 (d).

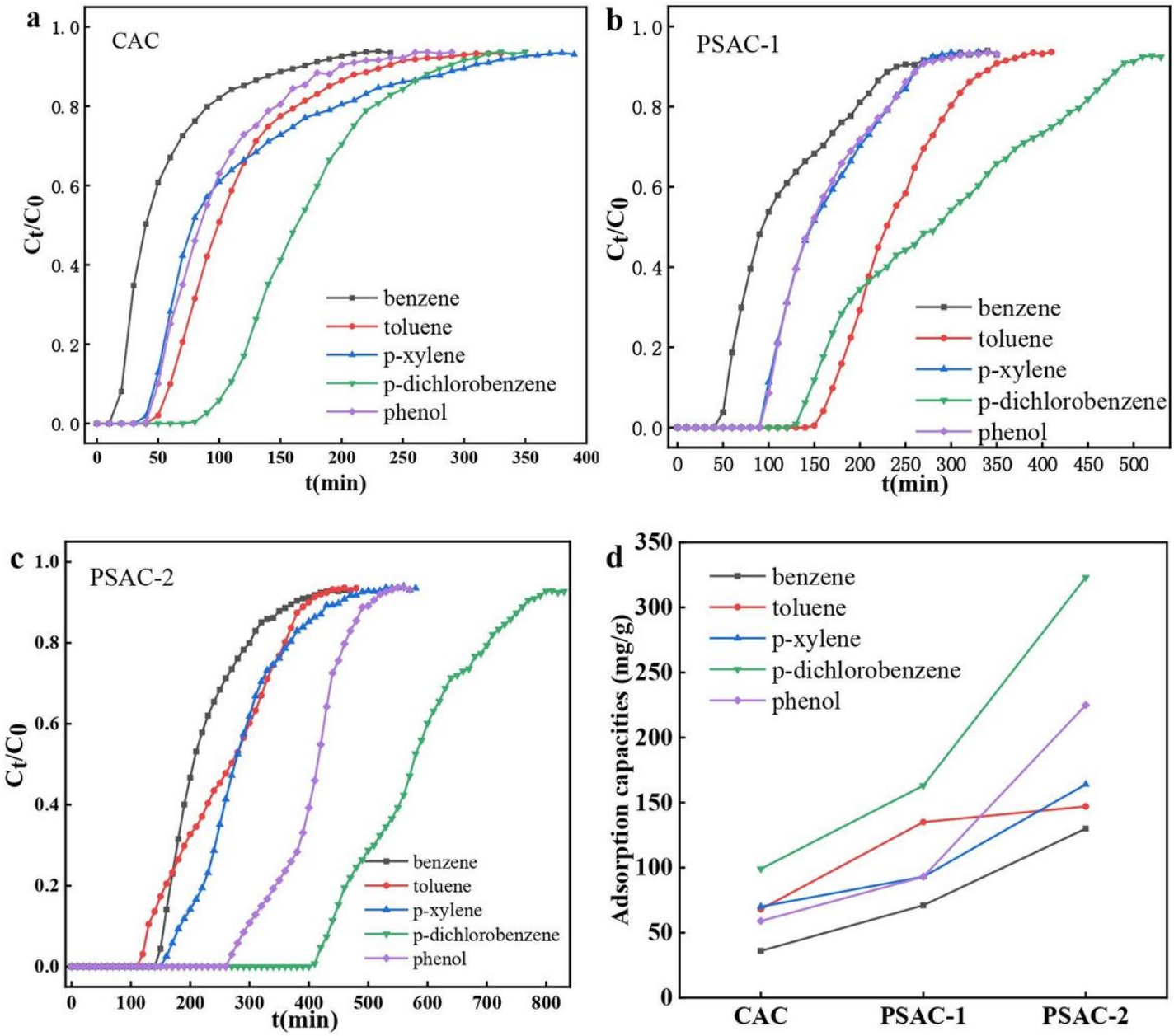

Figure 6

Breakthrough curves of VOCs adsorption by CAC (a), breakthrough curves of VOCs adsorption by PSAC-1 (b), breakthrough curves of VOCs adsorption by PSAC-2 (c) and the corresponding adsorption capacities (d).

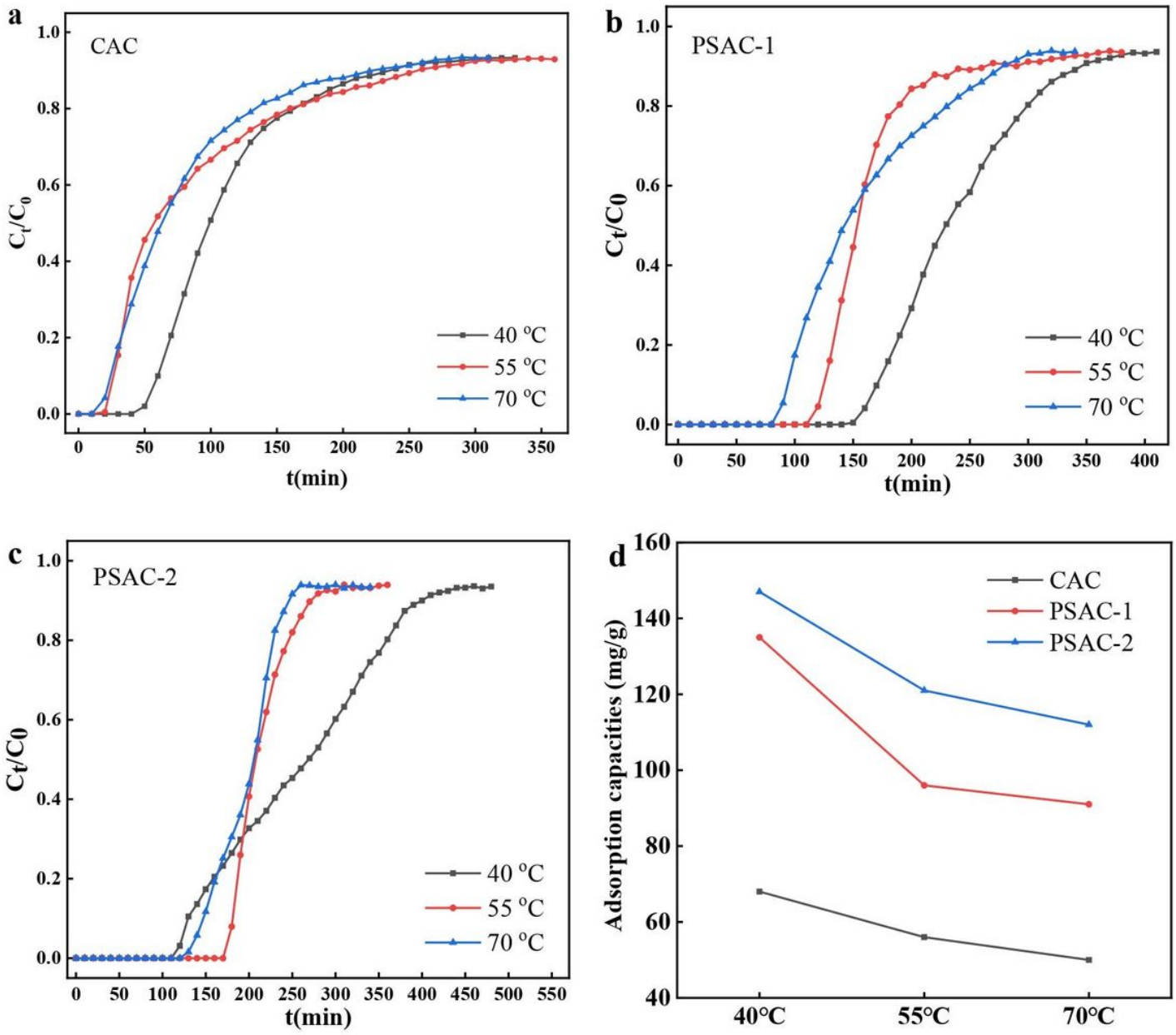

Figure 7

Breakthrough curves of toluene adsorption by CAC under different temperature (a), breakthrough curves of toluene adsorption by PSAC-1 under different temperature (b), breakthrough curves of toluene adsorption by PSAC-2 under different temperature (c) and the corresponding adsorption capacities (d).

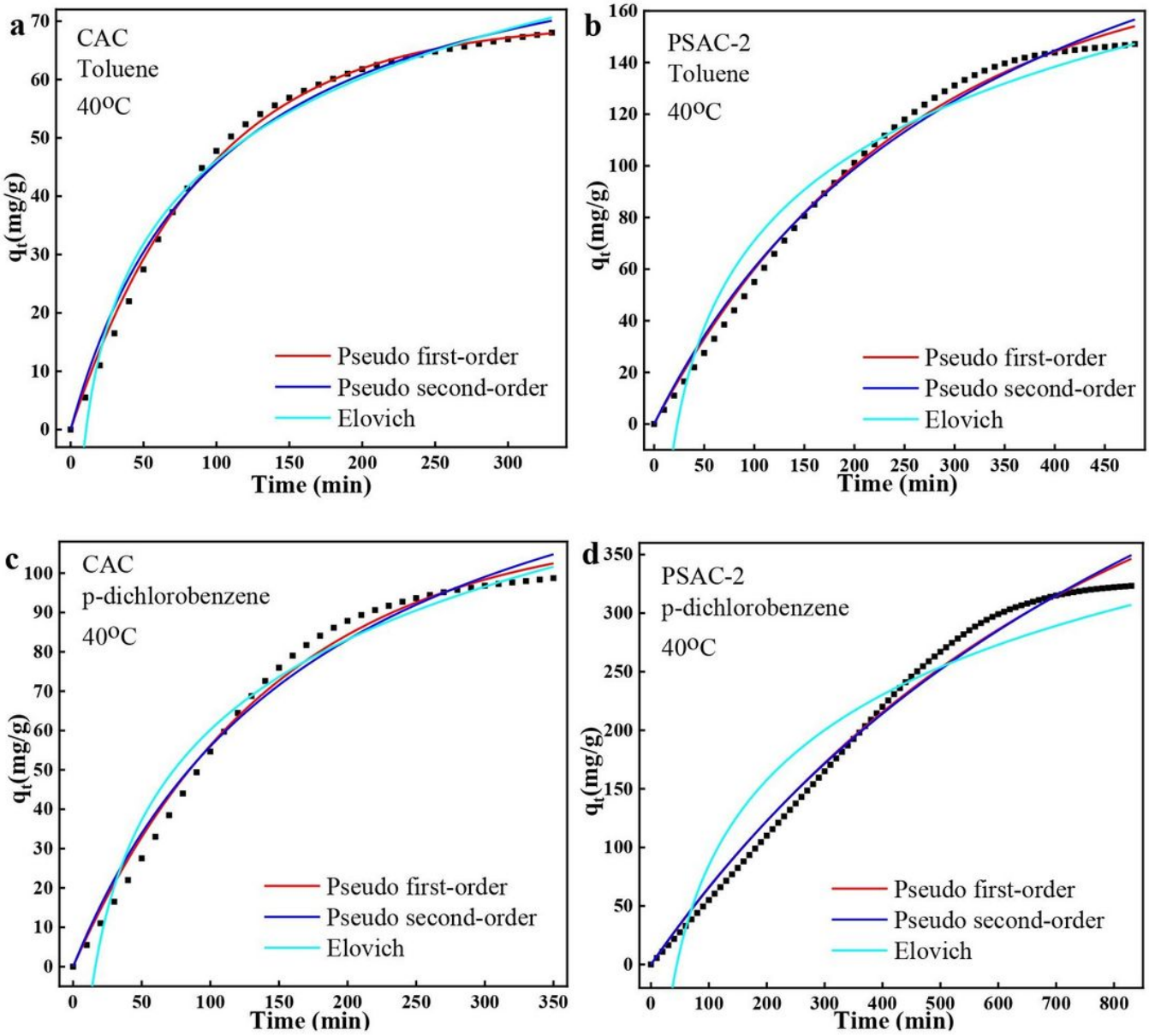

Figure 8

Nonlinear fitting curves of three kinetic models. Fitting curves of toluene adsorption process by CAC (a). Fitting curves of toluene adsorption process by PSAC-1 (b). Fitting curves of p-dichlorobenzene adsorption process by CAC (c). Fitting curves of p-dichlorobenzene adsorption process by PSAC-1 (d).

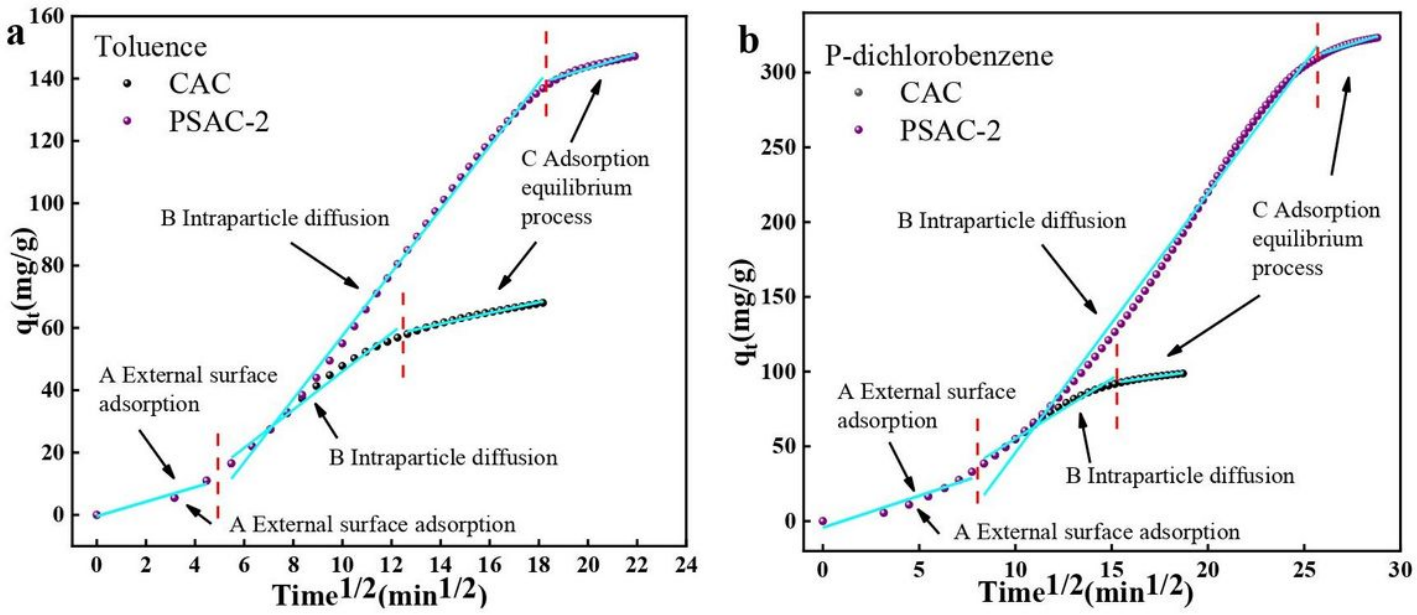

Figure 9

Intraparticle diffusion kinetic plots for toluene and p-dichlorobenzene adsorption. Fitting of toluene adsorption processes at CAC and PSAC-1, respectively (a). Fitting of p-dichlorobenzene adsorption processes at CAC and PSAC-1, respectively (b).

Supplementary Files

This is a list of supplementary files associated with this preprint. Click to download.

- GraphicalAbstract.jpg